

1
2
3
4
5
6
7
8
9
10
11
12
13
14
15
16
17
18
19
20
21
22

Investigating the effect of ballasting by CaCO_3 in *Emiliana huxleyi*: I.
Formation, settling velocities and physical properties of aggregates

Anja Engel^{1,2}, Jennifer Szlosek^{1,2}, Lynn Abramson², Zhanfei Liu², and Cindy Lee²

¹ Present address: Alfred Wegener Institute for Polar and Marine Research, 27515
Bremerhaven, Germany

²School of Marine and Atmospheric Sciences, Stony Brook University, Stony Brook, NY
11794-5000, USA

¹To whom correspondence should be addressed.

23 Abstract

24

25 To investigate the role of ballasting by biogenic minerals in the export of organic matter
26 in the ocean, a laboratory experiment was conducted comparing aggregate formation and settling
27 velocity of non-calcifying and calcifying strains of the coccolithophore *Emiliana huxleyi*.
28 Experiments were conducted by making aggregates using a roller table and following aggregate
29 properties during incubation for a period of 40 days. Size, shape and settling velocities of
30 aggregates were described by image analysis of video pictures recorded during the roller tank
31 incubation. Our results show that biogenic calcite has a strong effect on the formation rate and
32 abundance of aggregates and on aggregate properties such as size, excess density, porosity, and
33 settling velocity. Aggregates of calcifying cells (AGG_{CAL}) formed faster, were smaller and had
34 higher settling velocities, excess densities, and mass than those of non-calcifying cells
35 (AGG_{NCAL}). AGG_{CAL} showed no loss during the duration of the experiment, whereas AGG_{NCAL}
36 decreased in size after one month of incubation. Potential mechanisms that can explain the
37 different patterns in aggregate formation are discussed. Comparison of settling velocities of
38 AGG_{CAL} and AGG_{NCAL} with aggregates formed by diatoms furthermore indicated that the ballast
39 effect of calcite is greater than that of opal. Together these results help to better understand why
40 calcite is of major importance for organic matter fluxes to the deep ocean.

41

42

43

44

45

46

47

48 **Keywords: Ballast, coccolithophores, aggregates, settling velocity, excess density,**

49 1. Introduction

50
51 Quantifying rates of organic matter (OM) flux to the deep ocean and understanding the
52 mechanisms of this transport are necessary for fully predicting the ocean's role in the
53 sequestration of atmospheric CO₂. It is now well documented that the amount of OM that is
54 produced at the sea surface and exported from the surface ocean as sinking particles decreases
55 exponentially with depth; Very little material is exported below 1500 m and excluded from
56 exchange with the atmosphere for >1000 years (Suess, 1980; Martin et al., 1987, Antia et al.,
57 2001). To quantify OM fluxes, numerical models often apply algorithms that relate deep export
58 of OM to primary or new production. But what are the mechanisms responsible for the shape of
59 the export curve? Recently, a number of studies questioned whether OM fluxes can be
60 mechanistically (and thus mathematically) related directly to primary production (Armstrong et
61 al., 2002; François et al., 2002; Klaas and Archer, 2002). Armstrong et al. (2002) showed
62 instead that mass fluxes to the deep ocean are related to the simultaneous export of mineral
63 particles, and that the ratio of organic carbon to mineral fluxes ($F_{\text{POC}}:F_{\text{MIN}}$) in particulate matter
64 is about 0.05 and rather constant below a depth of 1800m. Klaas and Archer (2002) further
65 demonstrated that most of this association with organic carbon (as measured at 52 locations
66 around the world) is present in association with CaCO₃. Thus, deep fluxes of organic carbon and
67 CaCO₃ are tightly related, indicating that organisms with calcite shells such as coccolithophores
68 and foraminifera are of special importance for carbon export.

69 One explanation for the general importance of mineral fluxes for OM export to the deep
70 sea is that the minerals may act as ballast, thereby increasing OM sinking velocity and hence the
71 depth to which OM is exported (Ittekkot and Haake, 1990). Clearly, the faster OM sinks, the
72 greater its chance to reach the deep sea without being remineralized or dissolved. To explain the
73 constancy of the relationship between F_{POC} and F_{MIN} at the deep sea, Armstrong et al. (2002)
74 suggested two possible mechanisms: 1) organic compounds may be physically protected against

75 microbial degradation by their association with minerals (e.g., Lee et al., 2000; Hedges et al.,
76 2001); and/ or 2) organic matter may glue mineral particles together, but if the particulate
77 organic carbon content becomes too low, particles may disintegrate, removing both POC and
78 minerals from observed fluxes. Experimental studies that explore the role of mineral ballast in
79 enhancing particle settling speed or on the decomposition of OM are scarce, however, and focus
80 on terrestrial minerals as the source of ballast (e.g., Hamm, 2002; Arnarson and Keil, 2005;
81 Passow and De la Rocha, 2006).

82 Cocolithophores are one of the dominant marine phytoplankton groups on earth, and a
83 natural association of mineral and organic matter. The cells produce CaCO_3 platelets, or
84 coccoliths, that combine to form an outer coccosphere. Cocolithophores often form massive
85 blooms in temperate and sub-polar oceans, especially at continental margins and shelf seas
86 (Raitos et al., 2006; Baumann et al., 2005). Settling velocities of single coccolithophore cells
87 are typically only a few cm d^{-1} , not much above settling velocities of uncalcified phytoplankton.
88 Because export rates of biogenic calcite are on the order of several hundred m d^{-1} (Honjo, 1996),
89 export of biogenic matter by coccolithophores must therefore involve repackaging of cells into
90 larger particles through zooplankton grazing and defecation or through physical aggregation.

91 Particle aggregation in the ocean (e.g., by collision and subsequent adhesion of individual
92 particles such as phytoplankton and bacterial cells, fecal pellets, clays and debris) occasionally
93 leads to the formation of macroscopic aggregates ('marine snow', or aggregates > 0.5 mm). The
94 sinking velocity of aggregates depends on their size and density and is usually 10 - 10^5 times
95 greater than the sinking velocity of individual components (Shanks and Trent, 1980; Alldredge
96 and Gotschalk, 1988; Gibbs, 1985). Thus, aggregate settling is mainly responsible for vertical
97 mass flux and drives much of the elemental cycling in the ocean (Fowler and Knauer, 1986;
98 Asper et al., 1992). Despite its importance for export processes and ocean biogeochemistry,
99 however, little is known about aggregate formation by coccolithophores or the effect of biogenic
100 calcite on aggregate settling velocities and physical properties.

101 We investigated whether: 1) biogenic calcite from the coccolithophore *E. huxleyi* acts as
102 a ballast, and thus increases the settling velocity of aggregates, and 2) the association between
103 biogenic calcite and OM can slow down OM decomposition. Both hypotheses were tested in
104 laboratory experiments by comparing calcifying and non-calcifying cells of *Emiliana huxleyi*.
105 Incubation experiments were performed in the dark using roller tanks to allow for aggregation
106 and continuous settling of aggregates over a period of one month. Here, we report the effect of
107 calcification on the formation of aggregates, their physical properties and settling velocity.
108 Effects on the decomposition of OM revealed by changes in the chemistry of dissolved and
109 particulate components are reported elsewhere in this issue (Engel et al., 2008).

110

111

112 2. Methods

113

114 2.1. *Experimental set-up*

115 Calcifying (CAL) (CCMP2112, Bigelow Laboratories) and non-calcifying (NCAL)
116 strains of *Emiliana huxleyi* cells were grown in batch culture in f/4 media (Guillard ,1975) as
117 described in detail in Engel et al. (2008). The pH of the cultures and the predominance of
118 calcifying or non-calcifying cells were monitored in each culture. When each culture reached
119 late exponential growth phase, it was divided and transferred to eight cylindrical Plexiglas tanks,
120 seven of 4.5-L volume and one of 10-L volume, and kept in the dark at 9°C. All tanks were
121 placed on roller tables (Shanks and Edmondson, 1989) that rotated at 0.66 rpm so that aggregates
122 were formed from the coccolithophore cultures (CAL and NCAL) under conditions that allowed
123 for continuous particle settling. Due to manpower limitations, incubation of the two cultures in
124 the roller tanks was performed sequentially, not at the same time. To simulate the sinking of
125 aggregates into deeper and hence more dilute waters, the concentration of suspended cells was
126 lowered before the actual experiment began. This was accomplished by removing tanks from the

127 roller table on day 5 and allowing larger particles to settle for 10 minutes. Then 3 L of
128 supernatant containing suspended cells were removed from each 4.5-L tank and replaced by aged
129 coastal seawater. In the 10-L tank, 6.3 L of the original supernatant were replaced. At this point,
130 the tanks were again placed on roller tables at a rotation speed of 0.66 rpm.

131 Experiments lasted 30 d in the smaller tanks, and 40 days in the 10-L tank. To perform
132 chemical analyses of the aggregates and of the suspended particles in the seawater surrounding
133 the aggregates, a total of seven samplings were performed using the smaller tanks. At each
134 sampling point one tank was harvested. The first sampling was conducted 4h after the tanks were
135 reintroduced to the roller table and corresponds to time zero (day 0). The following sampling
136 points were after 3, 6, 10, 16, 23, 30 days. Sampling of the tanks for chemical analysis is
137 described in detail in Engel et al. (2008). Physical properties of aggregates were recorded from
138 the 10-L tanks and determined as described below.

139 A follow-up experiment to compare the efficiency of aggregate formation of NCAL and
140 CAL was conducted using four different cell concentrations of each culture. NCAL and CAL
141 cultures were grown simultaneously and harvested at late exponential growth phase as described
142 above, diluted with $0.2\ \mu\text{m}$ filtered seawater (FSW) by 1:1, 1:2, 1:4 and 1:8 (culture:FSW) to a
143 final volume of 5L. The total volume of particles >2 μm at each dilution was determined with a
144 Coulter Counter. Each sample was then incubated in 4.5 L tanks on the roller table as described
145 above, but simultaneously. After three days aggregates were separated from each tank, and
146 particle abundance and volume concentration of the aggregated particulate fraction (AGG) and
147 of the suspended particles within the water surrounding the aggregates (SUSP) were determined
148 with a Coulter Counter as described in Engel et al. (2008).

149

150

151

152

153 *2.2. Determination of aggregate size and settling velocity*

154 The size of aggregates and their settling velocity within the roller tanks were determined
155 by video recording aggregates in a 10-L roller tank of 30 cm diameter and 15 cm height (Fig. 1).
156 We chose the 10-L tank for video capture, because its larger radius ensured that the range of
157 motion of the aggregates would not be disturbed by the walls of the tank. To prevent collision
158 between aggregates and the tank wall, the rotation speed furthermore had to be repeatedly
159 increased during the experiment to a maximum speed at day 40 of 1.25 rpm for NCAL and 2.38
160 rpm for CAL. Rotation speed was increased slowly, and at least 12 h before a new video record
161 was taken, to ensure homogeneous fluid velocities inside the tank.

162 Aggregates were observed for 10 min daily with a Sony Digital 8 DCR-TRV460 video
163 camera equipped with an 80-mm Macro lens. The observation area (x/y coordination grid) was
164 3.9 cm x 4.5 cm (height x width) at a distance of 5.5 cm from the center of the tank. A digital
165 time code was placed on every video picture with a temporal resolution of 1/100 s. Single
166 pictures were captured from the video on a PC using the software Pinnacle Studio Plus 700-PCI
167 and analyzed with the public domain Java image processing program ImageJ (written by Wayne
168 Rasband at the Research Services Branch, National Institute of Mental Health, Bethesda,
169 Maryland, USA). The following parameters of each aggregate were measured semi-
170 automatically: Topview area (A), length of the major axis (major), length of the minor axis
171 (minor), the x-feret diameter, and position in the x-y plane. The x-feret diameter (d_f) of an
172 aggregate is the largest size of the aggregate in the horizontal direction. For the orientation of an
173 aggregate within the field of view, d_f is equivalent to the largest dimension of the aggregate
174 perpendicular to the direction of sinking. The optical resolution of digitized pictures was 4.4×10^{-4}
175 mm^2 per pixel, giving a size detection limit of 35 μm . Analysis of images was performed every
176 second or third day. On each day of observation, at least 20 randomly chosen images were
177 analyzed for aggregate dimensions, and the settling velocity was determined for at least ten
178 randomly-chosen aggregates.

179 The visible volume of each aggregate (V) was calculated as the volume of an equivalent
 180 ellipsoid using major and minor length. The area perpendicular to the direction of fall (A_p) was
 181 calculated using the feret diameter (d_f) according to:

182

$$183 \quad (1) \quad A_p = \pi (d_f)^2 / 4$$

184

185 After an initial spinup time, solid body rotation for the water inside the roller tank is
 186 established (Tooby et al., 1977; Jackson, 1994). During solid body rotation, the angular velocity
 187 of the fluid is the same at any point inside the tank, and no laminar shear should be present. In
 188 this case, a particle that is settling or rising within the tank will perform a circular movement
 189 around a center (CC), whose location along the horizontal axis of the tank depends on the
 190 particle's settling velocity (Tooby et al., 1977) (Fig. 1). During our experiment the circular
 191 movement of aggregates was readily observed during the entire incubation. The sinking velocity
 192 (U_{AG}) of an aggregate can then be derived from its apparent velocity (U^*), which is the
 193 movement of the aggregate relative to the fluid (Fig. 1), as follows:

194

$$195 \quad (2) \quad U^* = \frac{\Delta y_{1,2}}{\Delta x_{1,2}}$$

196

$$197 \quad (3) \quad U_{AG} = U^* \overline{\omega x_{1,2}}$$

198

199 where $\Delta y_{1,2}$ and $\Delta x_{1,2}$ describe the vertical and horizontal displacement of the aggregate
 200 in the x-y plane with time ($t_{1,2}$), ω is the angular velocity of the fluid (s^{-1}) and $\overline{x_{1,2}}$ is the average
 201 position of the aggregates along the x-axis. Because the rotational speed of the tank was adjusted
 202 to keep the aggregates floating within the tank, the relative movement of the aggregate is slow

203 enough to keep the aggregates within the field of view for several seconds. The benefit of this
 204 approach is that it is not necessary to determine the whole path of the aggregates movement but
 205 only a smaller subsection of it. In this way the optical magnification of the aggregate during
 206 video recording can be higher, which leads to a better resolution of aggregate size and shape.
 207 Detailed information about the physics in the roller tank is given in Tooby et al. (1977) and
 208 Jackson (1994). For more information about the method for determining the settling velocity of
 209 an aggregate inside the roller tank see Engel and Schartau (1999).

210

211 *2.3. Calculated aggregate properties*

212 The excess density ($\Delta\rho_{AG}$) of individual aggregates was derived from their settling
 213 velocity (U_{AG} , cm s^{-1}). Theoretically, the settling velocity of an aggregate in fluid results from
 214 the balance between gravity and drag force (Alldredge and Gotschalk 1988), as:

215

$$216 \quad (4) \quad U_{AG} = (2g(\rho_{AG} - \rho_{fl})V / (C_D \rho_{fl} A_p))^{0.5}$$

217

218 where the acceleration due to gravity (g) is 981 cm s^{-2} , ρ is the density in g cm^{-3} of either the
 219 aggregate (ρ_{AG}) or of the fluid (ρ_{fl}), V the visible aggregate volume, C_D the dimensionless drag
 220 coefficient, and A_p the area of the aggregate perpendicular to the direction of the fall. The term
 221 $(\rho_{AG} - \rho_{fl})$ denotes the excess density ($\Delta\rho_{AG}$) of the aggregate. To calculate $\Delta\rho_{AG}$, we used
 222 equation 4 and the empirical formula of Alldredge and Gotschalk (1988) for the drag coefficient
 223 C_D at higher (>0.5) Reynolds numbers (Re):

224

$$225 \quad (5)$$

$$226 \quad C_D = 95 (Re)^{-1.85}$$

227

228 with $Re = dU/v$, where d is the particle diameter and v is the kinematic viscosity. The kinematic

229 viscosity of the fluid is the quotient of the dynamic viscosity (ξ) and the density of the fluid (ρ_{fl})
 230 and was calculated to be $0.01189 \text{ cm}^2 \text{ s}^{-1}$. The dynamic viscosity (ξ) of the fluid was derived
 231 from temperature and salinity after Dietrich et al. (1975) and calculated to be $0.0122 \text{ g cm}^{-1} \text{ s}^{-1}$.
 232 The value for $\Delta\rho_{AG}$ typically varies between 10^{-2} and $10^{-5} \text{ g cm}^{-3}$ for marine snow, which is up to
 233 four orders of magnitude lower than $\Delta\rho$ of single phytoplankton cells (Alldredge and Gotschalk,
 234 1988). This is due to the fact that aggregates are highly porous, and the density of an aggregate
 235 is given by the sum of the densities of the volume fraction occupied by fluid and by solid
 236 components. Hence, the excess density can be expressed as:

237

$$238 \quad (6) \quad \Delta\rho_{AG} = [(\rho_s (1-P)) + (\rho_{fl} P)] - \rho_{fl}$$

239

240 Knowing $\Delta\rho_{AG}$, the porosity (P) can be derived from Eq. 6 if the densities of the solid
 241 components (ρ_s) and of the fluid (ρ_{fl}) are also known:

242

$$243 \quad (7) \quad P = 1 - (\Delta\rho_{AG} / \Delta\rho_s)$$

244

245 The density of the fluid (ρ_{fl}) was calculated from temperature and salinity data according
 246 to UNESCO/ ICES/ SCOR/ IAPSO (1981) to $1.02605 \text{ g cm}^{-3}$ for both NCAL and CAL
 247 experiments. We assumed a density (ρ_{sCAL}) of 1.19 g cm^{-3} for calcified cells after Paasche
 248 (2001) and estimated a density (ρ_{sNCAL}) of 1.095 g cm^{-3} for non-calcified cells.

249

250 *2.4. Statistics*

251 Non-linear curve fits to data were performed using SigmaPlot 9.0 (SysStat). To
 252 determine the significance of the correlation coefficient (r^2), t -tests according to Fisher (in Sachs,
 253 1974) were performed. The experiments were compared by analyses of variance or covariance of

254 data (ANOVA, ANCOVA). Statistical significance was accepted for $p < 0.05$. To estimate the
255 methodological error of the image analysis we performed ten replicate measurements of
256 aggregate sizes and settling velocities for each of three aggregates randomly-selected from the
257 small, medium and large size pools in each experiment. Thus, we chose different starting and
258 end points for the settling path of each individual aggregate.

259

260

261 3. Results

262

263 3.1. Biological and chemical changes during the incubation

264 Detailed information about the biological and chemical changes during the incubation
265 experiments is given in Engel et al. (2008) and will be summarized here only briefly. Initial cell
266 concentrations (day 0) in the tanks as determined by Coulter Counter were $2.66 \times 10^6 \text{ mL}^{-1}$ for the
267 NCAL and $1.77 \times 10^6 \text{ mL}^{-1}$ for the CAL culture. The average size of the calcifying *E. huxleyi*
268 cells was 4.2- μm equivalent spherical diameter (ESD), slightly larger than the average size of
269 cells that lacked a coccosphere (ESD=3.7 μm). The total particle volume concentration (ϕ) of
270 both cultures was quite similar initially, yielding 11.52 ppm for NCAL and 11.48 ppm for CAL.
271 Thus, the lower cell abundance in CAL incubations was almost fully compensated by the larger
272 size.

273 During both NCAL and CAL incubations, the total particulate mass (including the slowly
274 sinking smaller, suspended particles, and the macroscopic aggregates) decreased substantially
275 over time. Together with quantitative and qualitative changes in various particulate components
276 during the experiment this demonstrated that particulate organic matter (POM) decomposed
277 during both CAL and NCAL incubations, although to a greater extent in NCAL. However,
278 particle mass in the aggregate fraction increased during both experiments, more in the CAL than
279 NCAL cultures, indicating that POM was better preserved in the aggregates than in the

280 suspended particles.

281 The pH of tank seawater decreased in both cultures during the experiment so that the
282 seawater became undersaturated with respect to CaCO_3 . In both incubations, all tanks were
283 initially saturated with dissolved oxygen and did not become anoxic or even hypoxic during
284 decomposition.

285

286

287 *3.2. Aggregate properties*

288 In general, aggregates that formed in NCAL cultures were fluffier, larger and varied more
289 greatly in size than CAL aggregates, which were smaller, more abundant and less porous (see
290 photos in Fig. 1). NCAL and CAL aggregates were significantly different with respect to all
291 parameters determined (diameter, volume, settling velocity and excess density) (ANOVA,
292 $p < 0.001$). Error estimates for the measured properties of aggregates that formed during both
293 experiments are given in Table 1. For each size class, the standard deviations of the
294 measurements were below 5% of the mean values for all parameters.

295

296 *3.2.1. Aggregate formation*

297 Within the first day of incubation numerous (>50) aggregates > 1 mm formed in the CAL
298 culture. After day 10, more than 200 aggregates per tank were observed for CAL during each
299 recording. In contrast, aggregation was delayed for 4 days in the tanks containing the NCAL
300 culture, and less than 10 aggregates > 1 mm were observed at day 4 and 5. After one week of
301 incubation the number of aggregates in NCAL increased to >20 . On each sampling day,
302 aggregates that formed in the 4.5-L tanks were compared visually with aggregates that formed in
303 the 10-L tank. We observed that aggregates formed in the smaller tanks were similar in size and
304 appearance to those formed in the large tank.

305

306 To investigate whether the faster aggregation observed in CAL incubations was
307 reproducible and related to the difference in cell calcification, we performed the follow-up
308 experiment described earlier, where CAL and NCAL cultures were incubated simultaneously.
309 Here, we observed a higher aggregated particle volume in CAL than in NCAL incubations after
310 3 days at all but the lowest concentrations, where no significant difference between the two
311 cultures was observed (Fig. 2). This shows that within a given time span the net fraction of
312 particles that are included in aggregates is higher in CAL, indicating that calcified cells
313 aggregate more efficiently than non-calcified cells. Thus, the follow-up experiment supported the
314 observation from the decomposition experiment that formation of visible aggregates occurs
315 faster in CAL.

316

317 *3.2.2 Size and shape*

318 In general, the median feret diameter (d_f) of AGG_{NCAL} was four times larger than that of
319 AGG_{CAL} , and the median volume almost 10 times greater (Table 2). Over the course of the
320 experiment the median size of AGG_{NCAL} increased from $d_f = 0.25$ cm on day 4 to about 0.88 cm
321 on day 23 and decreased significantly afterwards (t -test, $p < 0.001$) (Fig. 3a). In contrast, during
322 the whole experiment the median size of AGG_{CAL} was 0.19 cm with only a slight variation over
323 time of 0.04 cm (Table 2, Fig. 3b). Chemical analysis gave no indication of net degradation of
324 organic matter in either NCAL or CAL aggregates (Engel et al, 2008). Hence, the decrease of
325 median size in AGG_{NCAL} after day 23 of the experiment indicates disaggregation of larger
326 aggregates into smaller ones. This may point to microbial processing of the organic matter and
327 potential weakening of the attachment of particles, especially within AGG_{NCAL} . In contrast, any
328 removal of particulate matter from AGG_{CAL} was either balanced by simultaneous aggregation, or
329 particulate matter within AGG_{CAL} was better protected from disaggregation and degradation.
330 During both experiments, the shape of aggregates deviated from a sphere, and aggregates
331 resembled oblate rather than prolate ellipsoids. This was more pronounced for AGG_{NCAL} with an

332 overall median value of the major: minor axis ratio of 1.57, compared to 1.41 for AGG_{CAL} (Table
333 2).

334

335

336 3.2.3. *Settling velocities*

337 The settling velocities of aggregates that formed from NCAL and CAL *E. huxleyi* cells
338 were very different, both in absolute numbers and in development over time. Although smaller
339 in size, AGG_{CAL} had higher median and maximum settling velocities than AGG_{NCAL} (Table 2).
340 NCAL aggregates started with a daily median settling velocity of 0.22 cm s⁻¹. As NCAL
341 aggregates grew larger over time, their settling velocity increased to a maximum median value of
342 1.53 cm s⁻¹ on day 23. After day 23, settling velocities of AGG_{NCAL} decreased significantly until
343 the end of the experiment (*t*-test, *p*<0.001) (Fig. 4a). Settling velocities for AGG_{CAL} reached a
344 daily median value of 1.69 cm s⁻¹ on the first day of formation and did not change significantly
345 over time (Fig. 4b). Since settling velocity is primarily a function of aggregate size, it is
346 illustrative to compare the relationship between settling velocity and size for different types of
347 aggregates (Fig. 5). This shows that even within a comparable size range (0.1-0.2 cm), sinking
348 velocities of NCAL and CAL aggregates were significantly different (ANOVA, *p*<0.001,
349 *n*=147), with CAL being on average four times higher than NCAL. A power function, $U = a$
350 (ESD)^b, was fitted to the data to describe the relationship of settling velocity to the equivalent
351 spherical diameter for AGG_{NCAL} and for AGG_{CAL} (Table 3).

352 In general, the median value for the Reynolds number for AGG_{NCAL} was larger than for
353 AGG_{CAL} due to more of the larger aggregates observed during NCAL incubations (Table 2).
354 However, due to the higher settling velocity, Reynolds numbers of CAL aggregates were larger
355 at comparable size. Because the Reynolds number inversely affects the drag exerted on a
356 settling aggregate, the median drag coefficients (*C*_D) of NCAL aggregates were lower than for
357 CAL, but consequentially *C*_D values for AGG_{NCAL} were higher at comparable sizes.

358

359 *3.2.4. Excess densities and porosities*

360 Excess densities of aggregates were derived from measurements of settling velocity and
 361 size. Excess densities of aggregates that formed from calcified cells were in general about 1-2
 362 orders of magnitude higher than those AGG_{NCAL} and showed much higher variability (Table 2).

363 Over the course of the experiment the daily median $\Delta\rho_{AG}$ for AGG_{NCAL} decreased from an initial
 364 value of $5.84 \times 10^{-3} \text{ g cm}^{-3}$ on day 4 to $7.58 \times 10^{-5} \text{ g cm}^{-3}$ on day 12 and varied between these two
 365 median values thereafter, with no significant correlation with time (Fig. 6a). For AGG_{CAL} the
 366 daily median $\Delta\rho_{AG}$ varied between 2.98×10^{-2} and $4.54 \times 10^{-3} \text{ g cm}^{-3}$, and were not significantly
 367 correlated with time throughout the experiment (Fig. 6b).

368 Because aggregates are fractal objects, i.e., their solid volume scales to length with an
 369 exponent $D_3 < 3$, we would expect the excess density of an aggregate to decrease with increasing
 370 length ($\Delta\rho_{AG} \sim l^{D_3-3}$) (Engel and Schertau, 1999). During both CAL and NCAL experiments, $\Delta\rho_{AG}$
 371 was significantly related to the equivalent spherical diameter (ESD) of aggregates as a power
 372 function, $\Delta\rho_{AG} = a (\text{ESD})^{-b}$ (Table 3). For AGG_{CAL} , absolute values for $\Delta\rho_{AG}$ were higher, and
 373 variability in $\Delta\rho_{AG}$ more pronounced than for AGG_{NCAL} , mainly because of the smaller size of
 374 AGG_{CAL} (Fig. 7). At comparable sizes the excess densities of both types of aggregates were
 375 more similar, with $\Delta\rho_{AG}$ being on average 2.3 times greater for AGG_{CAL} than for AGG_{NCAL} . The
 376 higher excess density of AGG_{CAL} at comparable sizes of aggregates can be explained by the
 377 presence of coccoliths within the aggregates. Biogenic calcium carbonate has a density of
 378 approximately 2.71 g cm^{-3} in air (Ittekkot and Haake, 1990), which is about 2.5 times the density
 379 that we estimated for the non calcified *E. huxleyi* cells.

380 Another factor impacting $\Delta\rho_{AG}$ is the porosity (P) of an aggregate. Porosities of
 381 aggregates during this experiment varied around an overall median of 95.9% for CAL and 99.6%
 382 for NCAL (Fig. 8a, b). This in turn shows that the volume occupied by cells within an aggregate

383 was 10 times higher for CAL than for NCAL aggregates. Thus, aggregates that formed from
384 calcifying cells were 10 times more compact than those from non-calcifying cells. Because
385 porosity of fractal aggregates increases with size, the lower P values for AGG_{CAL} are, again,
386 mainly due to their smaller sizes.

387
388 The particulate excess mass, equivalent to the dry mass of an aggregate, was calculated as
389 the product of $\Delta\rho_{AG}$ and the aggregate volume (V). By relating excess mass to ESD as a power
390 function, $Mass = a (ESD)^{-b}$, a significant (*t*-test, $p < 0.001$) relationship between mass and size of
391 aggregates was observed during both incubations (Fig. 9, Table 3). Chemical analysis of
392 particulate components (Y=POC, PON, or TEP) and dry mass was performed on the bulk
393 aggregate fraction collected during the NCAL and CAL incubation at 7 different sampling days
394 (Table 4; see Engel et al. 2008). No significant temporal changes in the [Y]:[dry mass] ratio of
395 the aggregate fractions were observed during both, NCAL and CAL incubations (*t*-test), except
396 for a decrease in TEP in AGG_{CAL} during the first six days. To calculate the contribution of the
397 different Y-components to the individual aggregates, we averaged [Y]:[dry mass] ratios over
398 time and multiplied the mean values with the excess mass of individual aggregates, derived from
399 $\Delta\rho_{AG}$ and V. A power law relationship, $y = a (ESD)^{-b}$, was fitted to the obtained data (Table 3).

400

401

402

403 4. Discussion

404

405 4.1. Initial aggregate formation: role of particle stickiness

406 We observed very different aggregation patterns during the CAL and NCAL experiments.
407 Aggregates in CAL incubations formed earlier than in NCAL incubations, and were smaller but
408 more abundant (see photos in Fig. 1). Theoretical analyses of particle coagulation processes

409 predict that aggregate formation depends on the probability of particle collision and on
410 coagulation efficiency, or the efficiency with which two particles that collide adhere to each
411 other (McCave, 1984; Jackson, 1990). Particle collision rate is a function of particle
412 concentration, size and the mechanism by which particles are brought into contact, e.g. Brownian
413 motion, shear or differential settling of particles. Coagulation efficiency depends on both the
414 particle collision rate and on physical-chemical properties of the particle surface. We can safely
415 assume that the physical environment affecting the initial phase of aggregation, e.g., temperature
416 and shear, was the same during both experiments, as both experiment were conducted under the
417 same experimental conditions.

418 During the initial spin-up of the roller tank, shear rates within the tank are high and
419 diminish until solid body rotation is reached; i.e. after about 12h for this experiment. During this
420 time coagulation is dominated by collision of phytoplankton cells brought into contact through
421 shear (Tooby et al., 1977; Jackson, 1994). Coagulation of particles by shear is a function of the
422 volume concentration of particles (Kiørboe et al., 1990), and of the shape of particles. For
423 example, elongated particles have a higher relative surface area and may experience higher
424 collision rates than spherical particles of the same volume. During this study, the initial volume
425 concentration of particles and the shape of cells were quite similar during both experiments,
426 likely leading to similar initial collision rates.

427 The majority of macroscopic aggregates in CAL and all aggregates of NCAL formed
428 after 24h, i.e., after the initial spin-up time, when shear forces within the tank were already
429 negligible and when differential sedimentation was the dominant collision mechanism between
430 particles. However, a few aggregates in CAL appeared within the first hours of incubation when
431 coagulation by shear may have been dominating. The faster aggregate formation by CAL cells
432 during these first hours was likely due to differences in stickiness, i.e. differences in the chemical
433 interactions of particle surfaces that affect the coagulation efficiency. In water samples with
434 different types of particles it has been shown that coagulation efficiency increases with the

435 fraction of transparent exopolymer particles (TEP) (Dam and Drapeau, 1995; Engel, 2000),
436 which form from dissolved polysaccharides (Aldredge et al., 1993; Passow, 2002; Engel et al.,
437 2004). However, initial TEP concentration during NCAL and CAL experiments were similar
438 and even slightly higher for NCAL (Engel et al., 2008). Thus, TEP concentration was
439 presumably not responsible for the earlier aggregation of CAL cells.

440 In an experiment where aggregates were produced on a roller table from phytoplankton
441 cells with and without the addition of terrestrial minerals, Hamm (2002) observed that aggregate
442 formation rate was faster in all experiments where mineral particles were added. Prior work has
443 shown that mineral colloids coagulate in the presence of biopolymers released by phytoplankton,
444 especially polysaccharides (Wilkinson et al., 1997). Polysaccharides that attach to the mineral
445 surface could in turn enhance the stickiness of the whole particle by increasing the amount of
446 sticky sites. An analogous mechanism might explain the faster aggregate formation of CAL cells.
447 Coccoliths of *E. huxleyi* are partly covered by acidic polysaccharides at the time of their
448 production (de Jong et al., 1976; van Emburg et al., 1986). Coccolith polysaccharides (CP)
449 contain ester sulfate and uronic acid groups that bind Ca^{2+} (de Jong et al., 1979). In contrast to
450 non-calcifying *E. huxleyi*, calcified cells stain with Alcian Blue (Engel et al., 2004), indicating
451 the presence of CP layering around the coccoliths. This CP layering may enhance the stickiness
452 of CAL cells, potentially leading to higher coagulation rates than for NCAL.

453

454 4.2 Increase of aggregate size: role of collision efficiency

455 Initial aggregation begins with two particles that collide and stick together. Ongoing
456 particle aggregation leads to an increase in aggregate size over time. During aggregation,
457 particle size distribution within a water sample changes from high abundances of small particles
458 initially, to a composite of small suspended particles and of aggregates of different sizes,
459 although small suspended particles remain numerically dominant. In principle, the final size of
460 an aggregate is determined by the dynamic balance between aggregation and disaggregation. It

461 has been suggested that formation of aggregates continues as long as particle abundance is high
462 enough for growing aggregates to contact other particles (Dyer, 1989). Thus, maximum
463 aggregate size would be related to initial concentration of suspended particles. Earlier
464 experiments, however, failed to show this relationship (Milligan and Hill, 1998).

465 Laminar or turbulent shear of the fluid are physical factors that exert stress on an
466 aggregate and can induce disaggregation. In the ocean, however, at the size-scale of aggregates
467 turbulence-induced stresses are low relative to the strength of aggregates (Alldredge et al., 1990).
468 Hill (1998) hypothesized that the final size of aggregates is controlled by forces that act on
469 aggregates during settling. This sinking-induced stress may rip cells off the outer surface of an
470 aggregate, once the settling velocity has reached a critical value. We cannot test the ‘Hill-
471 hypothesis’ here, because we have no information on the strength of an *E. huxleyi* aggregate or
472 on the turbulent-induced stress in the vicinity to the aggregate.

473 Another factor that may control aggregate size is the scavenging efficiency (E), the
474 efficiency by which a large aggregate collects smaller suspended particle within its path of
475 settling. Depending on the permeability of the aggregate, the velocity of fluid passing through
476 the aggregate is slower than outside the aggregate. The resulting backpressure deflects the fluid
477 in the path of the settling aggregate and consequently the suspended particles in that fluid (Adler,
478 1981). The rate at which smaller particles are then scavenged by the aggregate is a function of
479 the aggregate size, its settling velocity and the thickness of the shear induced boundary flow
480 around the aggregate.

481 Comparing CAL and NCAL during this study showed that the median and maximum size
482 of aggregates was significantly smaller in CAL than in NCAL incubations (Table 2). CAL
483 aggregates also appeared to be more spherical and compact than those of NCAL. Whereas
484 aggregate size in NCAL incubations increased continuously with time to the centimeter scale,
485 leading to a relatively small total number of aggregates, CAL aggregates reached a final size
486 much faster (within a day) and stayed relatively small over time, but at a higher total abundance.

487 This shows that although initial concentration and size of suspended particles were similar
 488 initially, the dynamics of aggregate formation that evolved during CAL and NCAL incubations
 489 were very different.

490 To test the hypothesis that final size of aggregates during this study was related to
 491 differences in the scavenging efficiency, we calculated the scavenging efficiency, E , for CAL
 492 and NCAL aggregates using the equations given in Stolzenbach (1993), i.e.:

493

$$494 \quad (8) \quad E = \bar{N} / N_0 \pi R^2 U$$

495 where \bar{N} is the rate (s^{-1}) of particle scavenging by the aggregate, N_0 is the number of suspended
 496 particles within a volume comprising the aggregate, R (cm) is the radius of the aggregate (here:
 497 $d_p/2$), and U is the settling velocity ($cm\ s^{-1}$). The equation to calculate \bar{N} is:

498

$$499 \quad (9) \quad \bar{N} = N_0 Q (1 - \exp(-\lambda L))$$

500

501 with Q ($cm^3\ s^{-1}$) being the volume flow rate through the aggregate. For N_0 , we used the
 502 concentration of particles in the size range 2 to 60 μm equivalent spherical diameter (ESD),
 503 which were determined on 7 sampling points during the experiment using a Coulter Counter in
 504 the smaller rotating tanks (see Engel et al., 2008). Linear interpolation was used to derive N_0 for
 505 those days where aggregate measurements were performed but no Coulter Counter data was
 506 obtained. For aggregates with a ratio of size to permeability (κ), given as $\beta = R / \kappa^{1/2} > 2$, the
 507 volume flow is given by:

508

$$509 \quad (10) \quad Q = (9/2) \pi R^2 U \beta^{-2}$$

510

511 Hence the volume flow of liquid through an aggregate is related to its size, permeability and

512 settling velocity. To estimate the permeability of an aggregate, Stolzenbach (1993) and authors
 513 cited therein have used the approximation:

$$514 \quad (11) \quad \kappa = a_p^2 [16\phi^{1.5}(1 + 56\phi^3)]^{-1}$$

515

516 where the particulate volume fraction (ϕ) is given by $\phi = 1 - P$, and a_p is the radius (cm) of the
 517 suspended particle. The aggregate filter coefficient (λ) was approximated with:

518

$$519 \quad (12) \quad \lambda = \phi / a_p$$

520

521 and the path length through the aggregate (L) with:

522

$$523 \quad (13) \quad L \cong (3/2)R$$

524 These calculations showed that at comparable settling velocities, the rates of fluid volume
 525 passing through CAL aggregates were much lower than for NCAL (Fig. 10). Consequently a
 526 higher deflection of fluid streamlines occurred around CAL aggregates, and the number of small,
 527 suspended particles brought into contact with an aggregate was about 1-2 orders of magnitudes
 528 lower for CAL than for NCAL during most part of the experiment (Fig. 11). Again, if we look at
 529 aggregates with similar settling velocities, scavenging efficiencies were much lower for CAL
 530 aggregates than for NCAL (Fig. 12). Moreover, as the size and settling velocity of the NCAL
 531 aggregates increased during aggregation, the scavenging efficiency increased as well,
 532 compensating for the decreasing concentration of suspended particles (N_0) (Fig. 12). In
 533 summary, for the rather compact CAL aggregates that reached high settling velocity very early
 534 during the experiment, the chance of growing to larger sizes by continued aggregation was much
 535 lower than for the more porous NCAL aggregates.

536 The smaller size and lower porosity of aggregates in CAL incubations might be directly

537 related to the mineral content. Hamm (2002) and Passow and De La Rocha (2006) observed a
538 similar phenomenon of reduced aggregate size with increasing content of added minerals in
539 similar types of experiments. Hamm (2002) inoculated two diatom species with clay suspensions
540 of different concentration in rotating tanks. In all settings, aggregates formed faster with clay
541 addition, were smaller in size, and had higher excess densities than the pure cultures. Passow
542 and De La Rocha (2006) formed aggregates by combining diatom cultures, mixtures of copepod
543 culture detritus, and dead diatom cells, with the inorganic minerals illite and calcium carbonate.
544 They also observed an inverse relationship between aggregate mineral content and aggregate
545 volume and porosity. In our experiment biogenic calcite enhanced aggregate formation in a
546 similar way, leading to smaller but heavier aggregates.

547

548 4.3. *Settling velocities*

549 We observed significantly higher settling velocities of CAL aggregates than of NCAL,
550 both absolutely and relative to size (Table 2). Higher settling velocities of CAL aggregates were
551 due to lower porosity of aggregates and to higher mass of particles that formed the aggregates.
552 Due to the compactness and spherical shape of CAL aggregates, the area perpendicular to the
553 direction of fall was relatively small. Thus, CAL aggregates experienced lower drag forces than
554 NCAL aggregates, which is another factor favouring higher settling velocities. Direct
555 comparison of both types of aggregates therefore showed that at equal mass, particulate matter
556 settles faster in a CAL than in an NCAL aggregate.

557 Comparing settling velocities of aggregates formed in experimental systems with those
558 settling *in situ* is not straightforward. *In-situ* measurements may be biased by water movement,
559 i.e., displacement of aggregates within the settling path, or non-straight settling paths. Laboratory
560 aggregates, however, are influenced by the artificial environment in which they are produced,
561 e.g., lack of turbulence and high initial shear in the rotating tanks, or the continued collision of
562 aggregates with suspended particles at potentially higher rates than *in-situ*, resulting in

563 aggregates that are much larger than those observed in the field and therefore have higher
564 settling velocities. We therefore chose to compare only aggregates of similar and small size, i.e.
565 ~1mm diameter, which are frequently observed in the field as well as in experimental studies.

566 In terms of absolute numbers, settling velocities during the experiments were at the upper
567 end of values reported for similarly-sized aggregates in the field; aggregates of 1mm diameter
568 had settling velocities of ~180 m d⁻¹ for NCAL and ~1200 m d⁻¹ for CAL. Alldredge and
569 Gotschalk (1989) reported settling velocities of 50-200 m d⁻¹ for biogenic aggregates that formed
570 *in situ*. Gibbs (1985) measured settling velocities of estuarine flocs containing clays, and
571 reported ~248 m d⁻¹. Hamm (2002) observed settling velocities between 230 m d⁻¹ to 860 m d⁻¹
572 for <1mm diameter aggregates of diatoms without and with clay addition, respectively.
573 Ziervogel and Forster (2005) determined rates of 172-259 m d⁻¹ for ~1mm aggregates formed in
574 rotating tanks from naturally sedimented material. Asper and Smith (2003) reported that ~1mm
575 aggregates settling within the upper 300 m of the Ross Sea (Antarctica) had minimum rates of
576 288 m d⁻¹. These studies show a wide range of settling velocity data for aggregates of about 1
577 mm in diameter.

578 We propose that the dissimilarities in NCAL and CAL aggregate formation and
579 properties, such as settling velocity, are primarily due to the presence of calcium carbonate.
580 Taking this argument a step further we have evaluated the effect of mineral ballast in the form of
581 biogenic calcite vs. biogenic silicate as produced by diatoms, by comparing the settling velocities
582 of aggregates obtained during this experiment with data gathered during earlier studies, where
583 the same methods for aggregate formation and settling velocity measurement were applied.

584 Data that are used for this comparison were obtained for aggregates formed from field
585 samples collected at 2 m depth during a diatom spring bloom in the coastal Baltic Sea in 1996
586 (n=338) (Engel, 1998), from field samples collected at 2m depth during a diatom spring bloom in
587 the northern Adriatic Sea in 1996 (n=93) (Engel, 1998), and from cell cultures of the pennate
588 diatom *Nitzschia costatum* containing different amounts of TEP (n=307), (Engel and Schartau,

589 1999). As can be seen from Fig. 13, aggregates that formed from calcifying *E. huxleyi* were
590 clearly different from aggregates that formed primarily from diatom cells, as the former spanned
591 a smaller size range and had higher settling velocities than the latter at comparable size. Settling
592 velocities of diatom aggregates were more similar to NCAL aggregates and comparable to
593 previous findings of aggregate settling velocities shown above. Although both create biogenic
594 minerals, our results thus suggest that coccolithophores may affect formation and sinking of
595 aggregates more than diatoms.

596

597 4.4. Implications for export processes in the field

598 What do these results suggest for the export of aggregates containing calcified cells in the
599 field? First, aggregates observed in the field below 100 m depth typically are in the range of a
600 few mm in size (Hill, 1998; Dierks and Asper, 1997; Asper and Smith, 2003). Larger flocs, up
601 to a few cm, have been observed in the upper few meters of the water column at certain
602 locations, such as coastal southern California, and often contain chain-forming diatoms
603 (Alldredge and Gotschalk, 1988; 1989). Thus, aggregate sizes observed during this study,
604 especially those of the calcified *E. huxleyi* culture, are within the range of those found *in situ*.

605 There are no direct observations of aggregates formed during blooms of *E. huxleyi* in the
606 field that we know of. However, high export rates such as those inferred from mass fluxes
607 arriving in deep sediment traps right after *E. huxleyi* blooms strongly indicate repackaging of
608 cells into larger particles such as aggregates or fecal pellets (Honjo, 1996). Marine snow-sized
609 aggregates (> 0.5 mm) containing *E. huxleyi* and other coccolithophores have been observed in
610 trap material (Broese et al., 2000). Aggregation of *E. huxleyi* into marine snow was also
611 observed during a mesocosm bloom study (Engel et al., 2004). Nevertheless, we do not know if
612 the properties and composition of aggregates that are formed during *E. huxleyi* blooms in the
613 field resemble those formed from pure *E. huxleyi* cultures. Initial cell abundance during this
614 experiment was $2\text{-}3 \times 10^6$ cells ml^{-1} , which is above the range of naturally occurring cell

615 abundances; i. e. 10^3 - 10^5 cells ml⁻¹ for the continental Northeast Atlantic Ocean (Berge, 1962,
616 Lampert et al., 2002; Mikaelyan et al., 2005).

617 If our results are representative for the field, aggregates formed by calcifying *E. huxleyi*
618 are fast forming, fast settling, and very robust carriers for exporting particulate organic matter to
619 the deeper water column. Because the presence of biogenic calcite was the difference between
620 our two experiments, aggregates formed by other calcifying coccolithophore species, and
621 perhaps by calcifying cells in general including foraminifera (Sarmiento et al, 2004), may show
622 similar properties. The enhancement of settling velocity together with high stability of CAL
623 aggregates over a 40-day-period indicate that biogenic calcite indeed acts as a ballast and
624 accelerates the formation and export of aggregated organic matter. In contrast to aggregates
625 formed from calcified cells, AGG_{N_{CAL}} showed signs of disaggregation after three weeks when
626 their size and settling velocities decreased significantly. This could indicate that the association
627 between organic matter and calcite is stronger and more difficult to break than the association
628 between purely organic molecules. In consequence organic aggregates would be more likely to
629 undergo decomposition during their transport to the deep-ocean than aggregates that include
630 calcite, as suggested in Armstrong et al. (2002).

631

632

633

634 5. Conclusions

635 To summarize, we observed several effects of biogenic calcite on aggregates dynamics
636 that can contribute to the ‘ballast ratio effect’: 1. biogenic calcite enhanced aggregate formation
637 of phytoplankton cells, 2. aggregates containing biogenic calcite were more compact, and
638 showed higher excess densities and higher settling velocities, 3. cohesion of particles within
639 aggregates containing biogenic calcite was stronger than in non-calcified aggregates, protecting
640 the aggregates from disaggregation over a 40-d period. Since net disaggregation was not

641 observed in aggregates of calcifying cells during incubation, fast settling mineral organic
642 aggregates are likely to reach the deep sea without significant loss, contributing to the efficient
643 export of the associated organic matter. The effect of calcite on settling velocities of aggregates
644 was found to be higher than that of opal in comparable studies. Our findings may therefore
645 provide one explanation for Klaas and Archer's (2002) observations that most of the particulate
646 organic matter arriving at the deep sea is associated with biogenic calcite.

647

648

649

650 6. Acknowledgements

651 This work was supported by NSF grants OCE 01-36370 and 04-24845 (MedFlux) and by
652 the Helmholtz Association (HZ-NG-102). The first author was supported by the Max Kade
653 Foundation of New York. We also would like to thank Gillian Stewart for laboratory help and
654 Markus Schartau for fruitful discussion. This is publication AWI n-17025, MSRC 1355, and
655 MedFlux 16.

656

657

658 References

- 659 Adler, P. M., 1981. Streamlines in and around porous particles. *Journal of Colloid and Interfacial*
660 *Science*, 81, 531-535.
- 661 Alldredge A.L., Gotschalk C.C., 1988. *In situ* settling behavior of marine snow. *Limnology and*
662 *Oceanography* 33, 339-351.
- 663 Alldredge A.L., Gotschalk C.C., 1989. Direct observations of the mass flocculation of diatom
664 blooms: characteristics, settling velocities and formation of diatom aggregates. *Deep Sea*
665 *Research* 36, 159-171.
- 666 Alldredge, A.L., Granata, T.C., Gotschalk, C.C., Dickey, T.C., 1990. The physical strength of
667 marine snow and its implications for particle disaggregation in the ocean. *Limnology and*
668 *Oceanography* 35, 1415-1428.
- 669 Alldredge A.L., Passow U., Logan, B. E., 1993. The abundance and significance of a class of
670 large, transparent organic particles in the ocean. *Deep-Sea Research* 40, 1131-1140.
- 671 Antia, A. N., et al. 2001. Basin-wide particulate carbon flux in the Atlantic Ocean: Regional
672 export patterns and potential for atmospheric CO₂ sequestration, *Global Biogeochemical*
673 *Cycles*, 15(4), 845-862, 10.1029/2000GB001376.
- 674 Armstrong, R.A., Lee, C., Hedges, J.I., Honjo, S., Wakeham, S.G., 2002. A new, mechanistic
675 model for organic carbon fluxes in the ocean based on the quantitative association of
676 POC with ballast minerals. *Deep-Sea Research Part II* 49, 219-236.
- 677 Arnarson, T. S., Keil, R. G., 2005. Influence of organic-mineral aggregates on microbial
678 degradation of the dinoflagellate *Scrippsiella trochoidea*. *Geochimica Cosmochimica*
679 *Acta* 69, 2111–2117.
- 680 Asper, V.L., Deuser, W.G., Knauer, G.A., Lohrenz, S. E., 1992. Rapid coupling of sinking
681 particle fluxes between surface and deep ocean waters. *Nature* 357, 670-672.
- 682 Asper, V. L., Smith, W. O. Jr., 2003. Abundance, distribution and sinking rates of aggregates in
683 the Ross Sea, Antarctica. *Deep-Sea Research I*, 50, 131-150.

- 684 Baumann, K.-H., Andruleit, A., Böckel, B. Geisen, M., Kinkel, H., 2005. The significance of
685 extant coccolithophores as indicators of ocean water masses, surface water temperature,
686 and paleoproductivity: a review. *Paläontologische Zeitschrift* 79, 93-112.
- 687 Berge, G., 1962. Discoloration of the sea due to *Coccolithus huxleyi* 'bloom'. *Sarsia* 6: 29-41.
- 688 Broese, A.T.C., Ziveri, P., Honjo, S., 2000. Coccolithophore (-CaCO₃) flux in the Sea of
689 Okhotsk: seasonality, settling and alteration processes. *Marine Micropaleontology* 39,
690 179-200.
- 691 Dam H. G., Drapeau D. T., (1995) Coagulation efficiency, organic-matter glues and the
692 dynamics of particles during a phytoplankton bloom in a mesocosm study. *Deep-Sea Res.*
693 II. 42.1: 111-123.
- 694 De Jong E.W., Bosch L., Westbroek P., 1976. Isolation and Characterization of a Ca²⁺- binding
695 Polysaccharide associated with coccoliths of *Emiliana huxleyi* (Lohmann) Kamptner.
696 *European Journal of Biochemistry*, 70, 611-621.
- 697 De Jong E., van Rens, L., Westbroek, P., Bosch, L., 1979. Biocalcification by the marine
698 alga *Emiliana huxleyi* (Lohmann) Kamptner. *European Journal of Biochemistry*, 99,
699 559-567.
- 700 Diercks, A.R., Asper, V. L., 1997. *In situ* settling speeds of marine snow aggregates below the
701 mixed layer -Black Sea and Gulf of Mexico. *Deep-Sea Research I*, 44, 385-398.
- 702 Dietrich, G., Kalle, K., Kraus, W., Siedler; G. 1975. *Allgemeine Meereskunde*. Gebrüder
703 Borntraeger, Berlin, Stuttgart, 593 pp.
- 704 Dyer, K. R., 1989. Sediment processes in estuaries: future research requirements. *Journal of*
705 *Geophysical Research*, 94, 14327-14399.
- 706 Engel, A., 1998. *Bildung, Zusammensetzung und Sinkgeschwindigkeiten mariner Aggregate*.
707 *Berichte Institut für Meereskunde Kiel* 300, 146 pp.
- 708 Engel, A., Schartau, M., 1999. Influence of transparent exopolymer particles (TEP) on sinking
709 velocity of *Nitzschia closterium* aggregates. *Marine Ecology Progress Series* 182, 69-76.

- 710 Engel, A., 2000. The role of transparent exopolymer particles (TEP) in the increase in apparent
711 particles stickiness (α) during the decline of a diatom bloom. *Journal of Plankton*
712 *Research* 22, 485-497.
- 713 Engel, A., Delille, B., Jacquet, S., Riebesell, U., Rochelle-Newall, E., Terbrüggen, A.,
714 Zondervan, I., 2004. TEP and DOC production by *Emiliana huxleyi* exposed to different
715 CO₂ concentrations: A mesocosm experiment. *Aquatic Microbial Ecology* 34, 93-104.
- 716 Engel, A., Abramson, L., Szlosek, J., Liu, Z., Stewart, G., Hirschberg, D., Lee, C., 2008.
717 Investigating the effect of ballasting by CaCO₃ in *Emiliana huxleyi*: II. Decomposition
718 of particulate organic matter. *Deep-Sea Research II*, submitted.
- 719 François, R., Honjo, S., Krishfield, R., Manganini, S., 2002. Factors controlling the flux of
720 organic carbon to the bathypelagic zone of the ocean. *Global Biogeochemical Cycles* 16,
721 1087, doi: 10.1029/2001GB001722.
- 722 Fowler, S.W., Knauer, G. A., 1986. Role of large particles in the transport of elements and
723 organic compounds through the oceanic water column. *Progress in Oceanography* 16,
724 147-194.
- 725 Gibbs, R.J., 1985. Estuarine flocs: Their size, settling velocity and density. *Journal of*
726 *Geophysical Research* 90, 3249-3251.
- 727 Guillard, R.R.L., 1975. Culture of phytoplankton for feeding marine invertebrates. In: W. L.
728 Smith, W.L., Chanley, M [Eds.], *Culture of Marine Invertebrate Animals*. Plenum Press,
729 New York, p. 26-60.
- 730 Hamm, C.E., 2002. Interactive aggregation and sedimentation of diatoms and clay-sized
731 lithogenic material. *Limnology and Oceanography* 47, 1790-1795.
- 732 Hedges, J.I., Baldock, J.A., Gélinas, Y., Lee, C., Peterson, M., Wakeham, S.G., 2001. Evidence
733 for non-selective preservation of organic matter in sinking marine particles. *Nature* 409,
734 801-804.
- 735 Hill, P.S., 1998. Controls on floc size in the sea. *Oceanography* 11, 13-18.

- 736 Honjo, S., 1996. Fluxes of particles to the interior of the open ocean. In: Ittekkot, V., Schäfer, P.,
737 Honjo, S., Depetris, P.J. (Eds.), Particle Flux in the Ocean. SCOPE 57. Wiley and Sons
738 Ltd., Chichester, pp. 91-154.
- 739 Ittekkot, V., Haake, B., 1990. The terrestrial link in the removal of organic carbon. In: Ittekkpot,
740 V., Kempe, S., Michaelis, M., Spitzzy, A. (Eds.) Facets of Modern Biogeochemistry.
741 Springer, Berlin, pp. 319-325.
- 742 Jackson, G.A., 1990. A model of the formation of marine algal flocs by physical coagulation
743 processes. Deep-Sea Research I, 37, 1197-1211
- 744 Jackson, G.A., 1994. Particle trajectories in a rotating cylinder: implications for aggregation
745 incubations. Deep-Sea Research I, 41, 429-437.
- 746 Klaas, C., Archer, D.E., 2002. Association of sinking organic matter with various types of
747 mineral ballast in the deep sea: Implications for the rain ratio. Global Biochemical Cycles
748 16, 1116, doi: 10.1029/2001GB001765.
- 749 Kiørboe, T., Andersen, K. P., Dam, H. G., 1990. Coagulation efficiency and aggregate formation
750 in marine phytoplankton. Marine Biology 107, 235-245.
- 751 Lampert, L., Queuiner, B., Labasque, T., Pichon, A., Lebreton, N., 2002. Spatial variability of
752 phytoplankton composition and biomass on the eastern continental shelf of the Bay of
753 Biscay (north-east Atlantic Ocean). Evidence for a bloom of *Emiliania huxleyi*
754 (Prymnesiophyceae) in spring 1998. Continental Shelf Research 22, 1225-1247.
- 755 Lee, C., Wakeham, S.G., Hedges, J.I., 2000. Composition and flux of particulate amino acids
756 and chloropigments in equatorial Pacific seawater and sediments. Deep-Sea Research I,
757 47, 1535-1568.
- 758 Martin, J. H., Knauer, G. A., Karl, D. M., Broenkow, W.W., 1987. VERTEX; carbon cycling in
759 the Northeast Pacific Deep-Sea Research Part A 34, 2A, 267-285.
- 760 McCave, I.N., 1984. Size spectra of aggregation of suspended particles in the deep ocean. Deep-
761 Sea Research 31, 329-352.

- 762 Mikaelyan, A.S., Pautova, L.A., Pogosyan, S.I., Sukhanova, I.N., 2005. Summer Bloom of
763 Coccolithophorids in the Northeastern Black Sea. Russian Academy of Sciences.
764 Oceanology 45, 127-138. 2005.
- 765 Milligan, T.G., Hill, P.S., 1998. A laboratory assessment of the relative importance of
766 turbulence, particle composition, and concentration in limiting maximal floc size and
767 settling behaviour. Journal of Sea Research 39, 227-241.
- 768 Paasche, E., 2001. A review of the coccolithophorid *Emiliana huxleyi* (Prymnesiophyceae), with
769 particular reference to growth, coccolith formation, and calcification-photosynthesis
770 interactions. Phycologia 40. 503-529.
- 771 Passow, U., 2002. Transparent exopolymer particles (TEP) in aquatic environments., Progress in
772 oceanography 55, 287-333.
- 773 Passow, U., De La Rocha, C., 2006. The accumulation of mineral ballast on organic aggregates.
774 Global Biogeochemical Cycles 20, GB1013, doi:10.1029/2005GB002579.
- 775 Raitos D.E., Lavender, S.J. , Pradhan, Y. Tyrrell, T. Reid, P.C. Edwards, M., 2006.
776 Coccolithophore bloom size variation in response to the regional environment of the
777 subarctic North Atlantic. Limnology and Oceanography 51, 2122-2130.
- 778 Sachs, L., 1974. Angewandte Statistik. Springer Verlag Berlin Heidelberg New York.
- 779 Sarmiento, J.L., Dunne J., Armstrong, R.A., 2004. Do we now understand the ocean's biological
780 pump? U.S.JGOFS News 12: 1-5.
- 781 Shanks, A.L., Edmondson, E.W., 1989. Laboratory-made artificial marine snow: A biological
782 model of the real thing. Marine Biology 101, 463-470.
- 783 Shanks A.L., Trent, J.D., 1980. Marine snow: sinking rates and potential role in vertical flux.
784 Deep Sea Research 27, 137-143.
- 785 Stolzenbach, K., 1993. Scavenging of small particles by fast sinking porous aggregates. Deep-
786 Sea Research Part I 40, 359-369.
- 787 Suess, E., 1980. Particulate organic carbon flux in the oceans - surface productivity and oxygen

- 788 utilization. Nature 288, 260-263.
- 789 Tooby, P.F., Wick, G.L., Isaacs, J.D., 1977. The motion of a small sphere in a rotating velocity
790 field: a possible mechanism for suspending particles in turbulence. Journal of
791 Geophysical Research 82, 2096-2100.
- 792 UNESCO/ ICES/ SCOR/ IAPSO, 1981. Background papers and supporting data on the
793 international equation of state of seawater. UNESCO Technical Paper in Marine Science
794 (Paris), 38.
- 795 Van Emburg, P.R., De Jong, E.W., Daems, W.T.H., 1986. Immunochemical localization of a
796 polysaccharide from biomineral structures (coccoliths) of *Emiliana huxleyi*. J Ultrast
797 Mol Struc Re. 94, 246-25.
- 798 Wilkinson, K. J., Joz-Roland, Buffle, J., 1997. Different roles of pedogenic fulvic acids and
799 aquatic biopolymers on colloid aggregation and stability in freshwaters. Limnology and
800 Oceanography 42, 1714-1724.
- 801 Ziervogel, K., Forster, S., 2005. Aggregation and sinking behaviour of resuspended fluffy layer
802 material. Continental Shelf Research 25, 1853-1863.
- 803

804 Figure legends:

805 Figure 1: Sketch of the experimental set-up to record aggregate properties during the
806 experiment. The camera observes a section of the roller tank (shaded area). During solid body
807 rotation of the fluid inside the tank, the settling velocity (U_{AGG}) of an aggregate that moves on a
808 circular path around a center (cc) and from point (y_1, x_1) at t_1 to the point (y_2, x_2) at t_2 can be
809 determined using Eqs. 2 and 3. For details see text. Photographs taken from the roller tanks at
810 day 12 of the two experiments showed the different morphology of aggregates that formed from
811 non-calcified and calcified cells. Size bar: 1cm.

812
813 Figure 2: Results of the follow-up roller table experiment to compare the efficiency of
814 aggregation in CAL and NCAL. Depicted is the total particle volume of aggregates (>1 mm) per
815 litre of tank water after 3 days of roller table incubation relative to the total initial volume of
816 particles >2 μm ESD. Open circles, NCAL, solid circles, CAL. Also shown are the data of the
817 decomposition experiment: open triangle, NCAL, solid triangle, CAL.

818
819 Figure 3a, b: Box plots of the feret diameter (d_f) of aggregates during the course of the
820 decomposition experiments. A) NCAL incubations, b) CAL incubations. Each box encloses
821 50% of the data with the median value of the variable displayed as a line. The bottom of the box
822 marks the 25% limit, and the top the 75% limit, of the variable population. The lines extending
823 from the top and bottom of each box marks the minimum and maximum values within the data
824 set. The white line indicates the mean value.

825

826

827 Figure 4a, b: Settling velocity of aggregates during the course of the decomposition
828 experiments. A) NCAL incubations, b) CAL incubations. For box plot definition see Fig. 3.

829

830 Figure 5: Relationship between settling velocity and equivalent spherical diameter (ESD)
831 of aggregates. Light circles, NCAL; dark circles, CAL.

832

833 Figure 6 a, b: Box plots of the excess density of aggregates over the course of the
834 experiment. A) NCAL incubations, b) CAL incubations. For box plot definition see Fig. 3. Note
835 different scaling on y-axis.

836

837 Figure 7: Excess density of aggregates and relation to the equivalent spherical diameter
838 (ESD) of aggregates. Light circles, NCAL; dark circles, CAL

839

840 Figure 8a, b: Box plots of the porosity of aggregates over the course of the experiment.
841 A) NCAL incubations, b) CAL incubations. For box plot definition see Fig. 3.

842

843 Figure 9: Mass of aggregates and relation to the equivalent spherical diameter (ESD) of
844 aggregates. Light circles, NCAL; dark circles, CAL.

845

846 Figure 10: Estimated volume flow (Q) through aggregates related to the observed settling
847 velocities of aggregates. Light circles, NCAL; dark circles, CAL.

848

849

850 Figure 11a, b: Number of suspended small particles (\bar{N}) brought into contact with
851 aggregates over the course of both experiments. A) NCAL incubations, b) CAL incubations. For
852 box plot definition see Fig. 3.

853

854 Figure 12: Estimated scavenging efficiency (E) of aggregates as related to aggregate feret
855 diameter and settling velocity. Light circles, NCAL; dark circles, CAL.

856
857 Figure 13: Settling velocities of aggregates formed by calcified and non-calcified cultures
858 of *E. huxleyi* (solid and open circles) in comparison to aggregates formed from a culture of the
859 pennate diatom *Nitzschia closterium* (open triangle) and to aggregates from field samples
860 during diatom blooms in the coastal Baltic Sea (rectangles) and at the northern Adriatic Sea
861 (gray triangles).
862

863 Table 1: Error calculation for parameters obtained from image analysis of aggregates that formed
 864 from a non-calcified (NCAL) and a calcified (CAL) strain of the coccolithophore *E. huxleyi*
 865 during incubation in roller tanks. Errors are the standard deviations of the mean values of ten
 866 replicate measurements from one randomly selected aggregate each of small (s), medium (m)
 867 and large (l) size. Values are given in %. Symbols are defined in the text.

	Cal_s	Cal_m	Cal_l	Avrg_{Cal}	NCAL_s	NCAL_m	NCAL_l	Avrg_{NCAL}	Avrg_{total}
Symbol									
U	2.71	1.88	2.58	2.39	5.14	3.60	1.48	3.41	2.94
d _f	4.76	2.56	3.07	3.46	0.84	0.82	0.61	0.76	1.58
V	4.24	6.63	7.43	6.10	2.44	2.23	3.08	2.58	4.36
Re	5.34	3.69	5.40	4.81	5.44	4.05	1.59	3.69	4.03
$\Delta\rho_{AG}$	3.7	6.11	6.79	5.53	1.84	1.77	3.04	2.22	3.7
P	0.47	0.27	0.13	0.29	0.27	0.01	0.02	0.10	0.47

868 Table 2: Parameter statistics for NCAL and CAL aggregates that formed during the roller tank
 869 incubations. Number of observations: NCAL=268, CAL=136, SD=standard deviation. Symbols
 870 are defined in the text.

Symbol	Unit	Incubation	Median	SD	min	max
d_f	cm	NCAL	0.85	0.34	0.13	1.55
		CAL	0.19	0.04	0.09	0.29
V	10^{-3} cm^3	NCAL	65	91	0.28	459
		CAL	0.81	0.89	0.19	7.0
ESD	cm	NCAL	0.54	0.21	0.08	1.1
		CAL	0.12	0.03	0.07	0.24
U	cm s^{-1}	NCAL	1.1	0.45	0.10	2.1
		CAL	1.8	0.26	1.1	2.5
$\Delta\rho_{AG}$	$10^{-3} \text{ g cm}^{-3}$	NCAL	0.13	1.3	0.02	15
		CAL	12	8.0	2.1	41
P	1	NCAL	0.996	0.04	0.649	0.999
		CAL	0.959	0.03	0.858	0.993
major:minor	1	NCAL	1.6	0.44	1.0	4.7
		CAL	1.4	0.31	1.0	2.6
Re	$\text{cm g}^{-1} \text{ s}^{-2}$	NCAL	79	54	2.3	250
		CAL	26	10	12	65
C_D	1	NCAL	0.03	2.2	0.10	20
		CAL	0.28	0.19	0.04	1.2

871

872

873

874 Table 3: Regression statistics for the power law curve fit $y=a(x)^b$, with $x = \text{ESD (cm)}$, of
 875 various variables determined for aggregates of NCAL and CAL. Significance level for all
 876 coefficients was $p<0.001$. SD= standard deviation, number of observations: NCAL=268,
 877 CAL=136.

y	Exp.	a	SD	b	SD	r²
U (cm s ⁻¹)	NCAL	1.94	0.042	0.89	0.04	0.79
	CAL	3.51	0.327	0.33	0.05	0.30
Mass (μg)	NCAL	12.7	0.06	0.30	0.01	0.91
	CAL	13.9	0.29	0.21	0.01	0.76
POC (μg)	NCAL	6.03	0.03	0.30	0.01	0.91
	CAL	2.48	0.05	0.21	0.01	0.76
PON (μg)	NCAL	0.51	0.03	0.30	0.01	0.91
	CAL	0.23	0.005	0.21	0.01	0.76
TEP (μg C)	NCAL	0.025	0.0001	0.30	0.01	0.91
	CAL	0.30	0.006	0.21	0.01	0.76
$\Delta\rho_{AG}$ (g cm ⁻³)	NCAL	3.17×10^{-5}	3.22×10^{-7}	-2.53	0.05	0.92
	CAL	2.61×10^{-5}	6.6×10^{-7}	-2.80	0.01	0.99

878

879

880

881

882

883

884

885

886

887

888

889

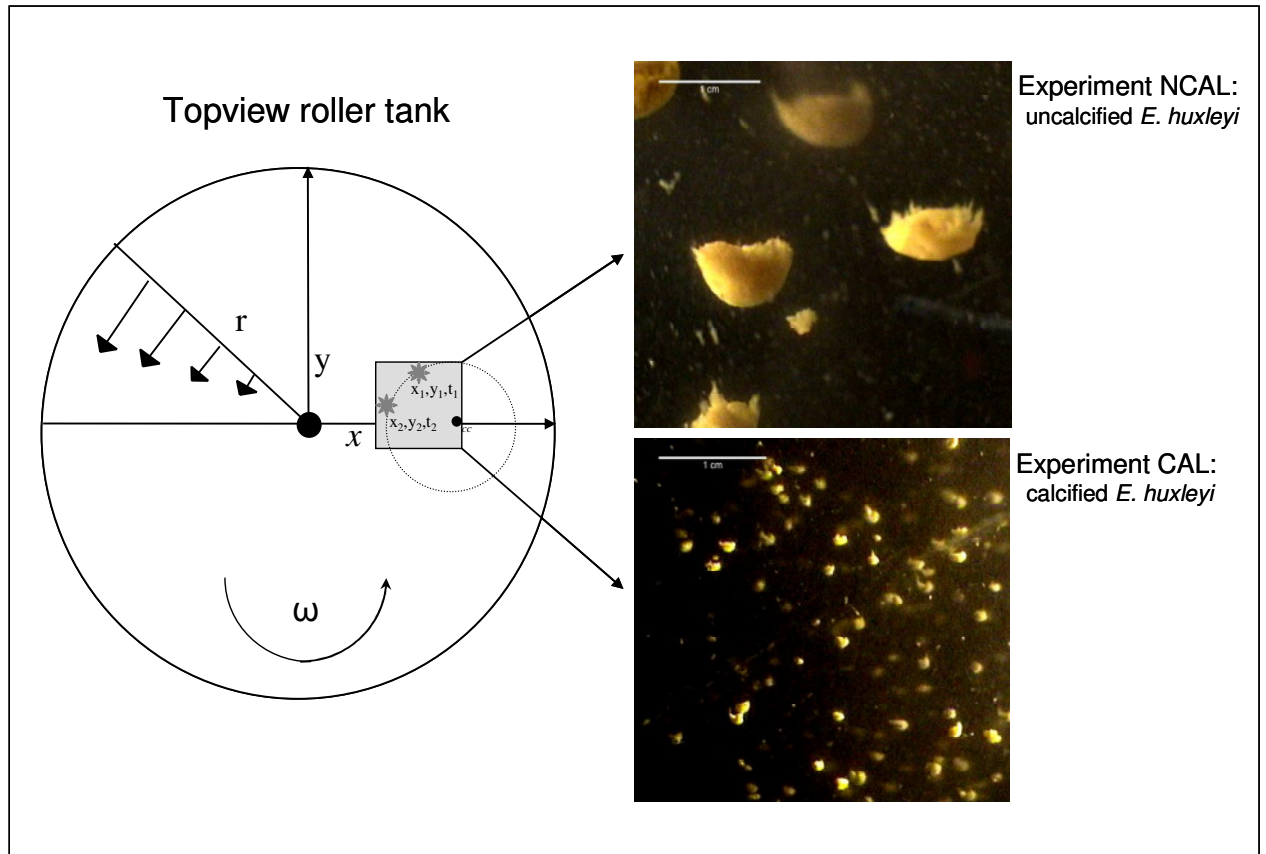
890

891 Table 4: Ratios (g:g) between organic components and mass of particulate matter within
 892 aggregates obtained by chemical analysis of the bulk aggregate fraction on several days during
 893 the decomposition experiment with non-calcifying (NCAL) and calcifying cells (CAL) of *E.*
 894 *huxleyi*.

day	POC:mass		PON:mass		TEP:mass	
	NCAL	CAL	NCAL	CAL	NCAL	CAL
1	-	0.14	-	1.8×10^{-2}	-	5.1×10^{-2}
3	-	0.11	-	1.1×10^{-2}	-	4.2×10^{-2}
6	0.44	0.15	4.2×10^{-2}	1.4×10^{-2}	2.4×10^{-2}	1.0×10^{-2}
10	0.44	0.15	3.8×10^{-2}	no data	1.6×10^{-2}	1.9×10^{-2}
16	0.56	0.17	4.4×10^{-2}	1.3×10^{-2}	1.5×10^{-2}	1.4×10^{-2}
23	0.52	0.20	4.3×10^{-2}	1.8×10^{-2}	3.9×10^{-2}	1.4×10^{-2}
30	0.42	0.15	3.5×10^{-2}	1.7×10^{-2}	2.4×10^{-2}	1.6×10^{-3}

895

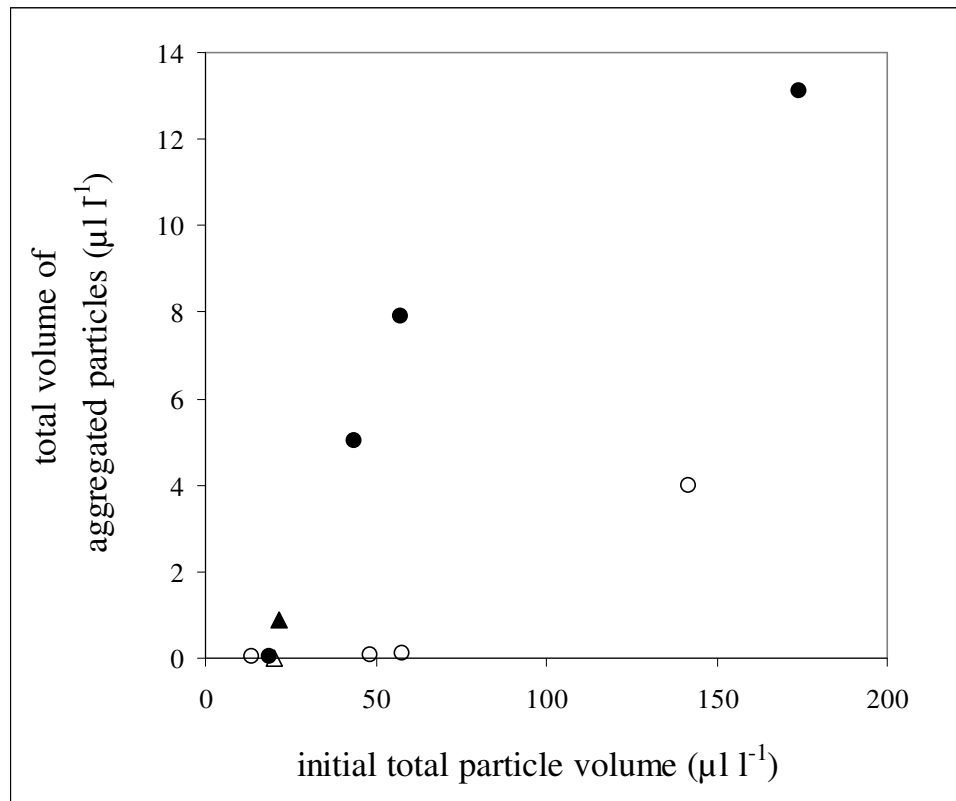
896
897
898
899
900
901
902
903
904
905
906
907
908
909
910
911
912
913
914
915
916
917
918
919
920
921



Engel et al. Figure 1

922

923



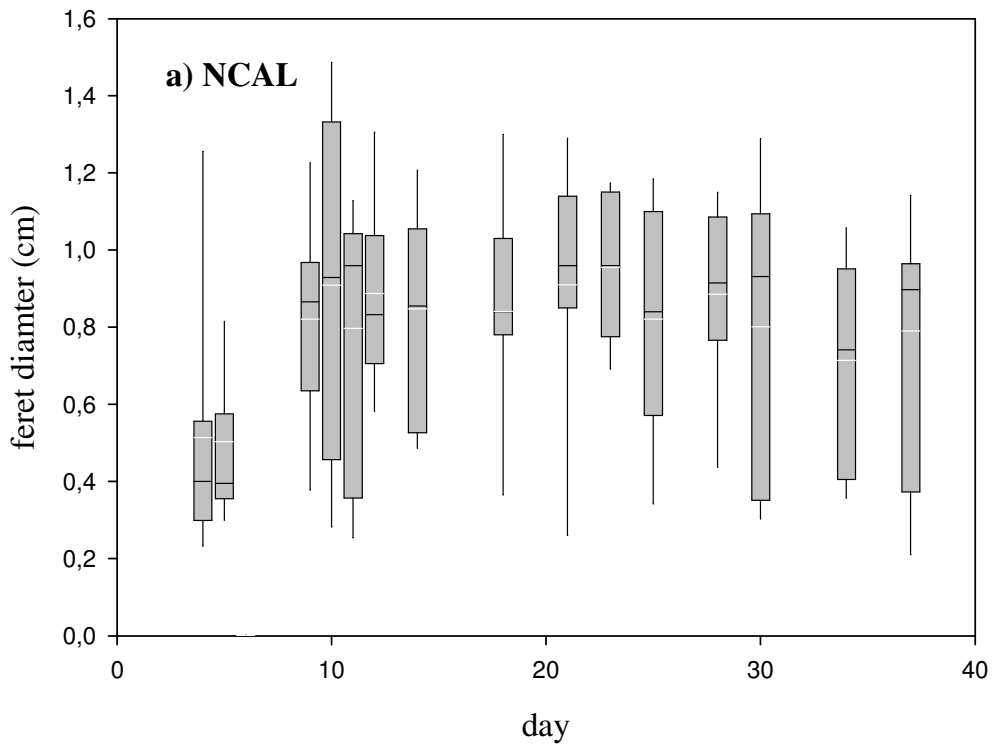
924

925

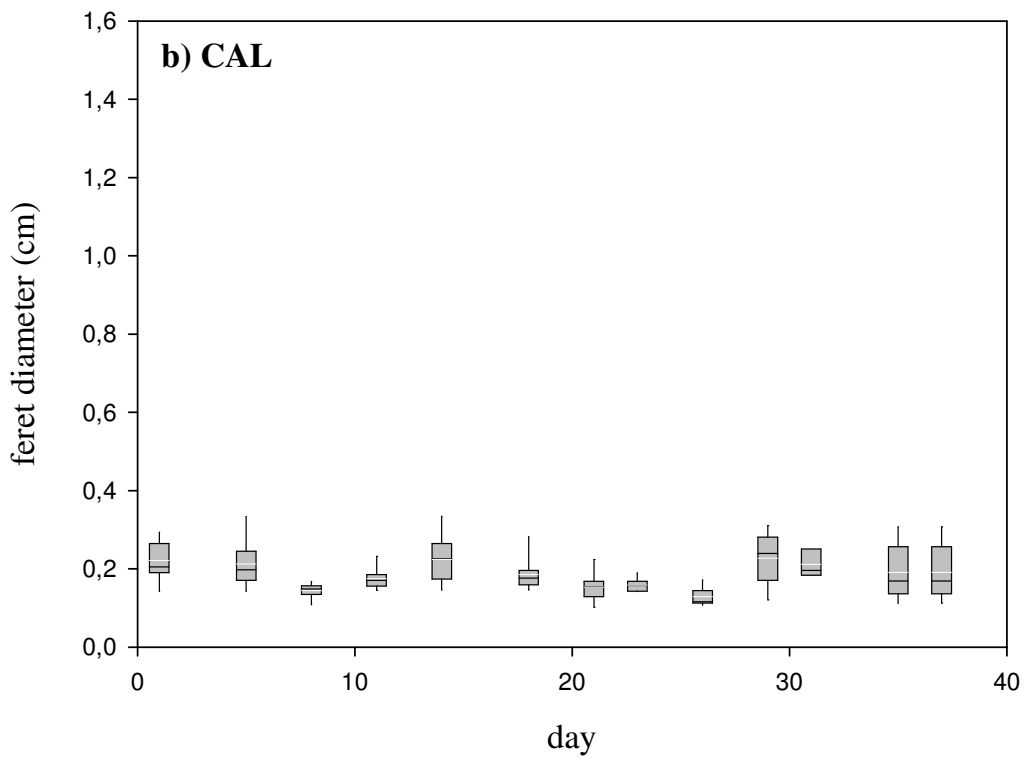
926

927

Engel et al. Figure 2



928



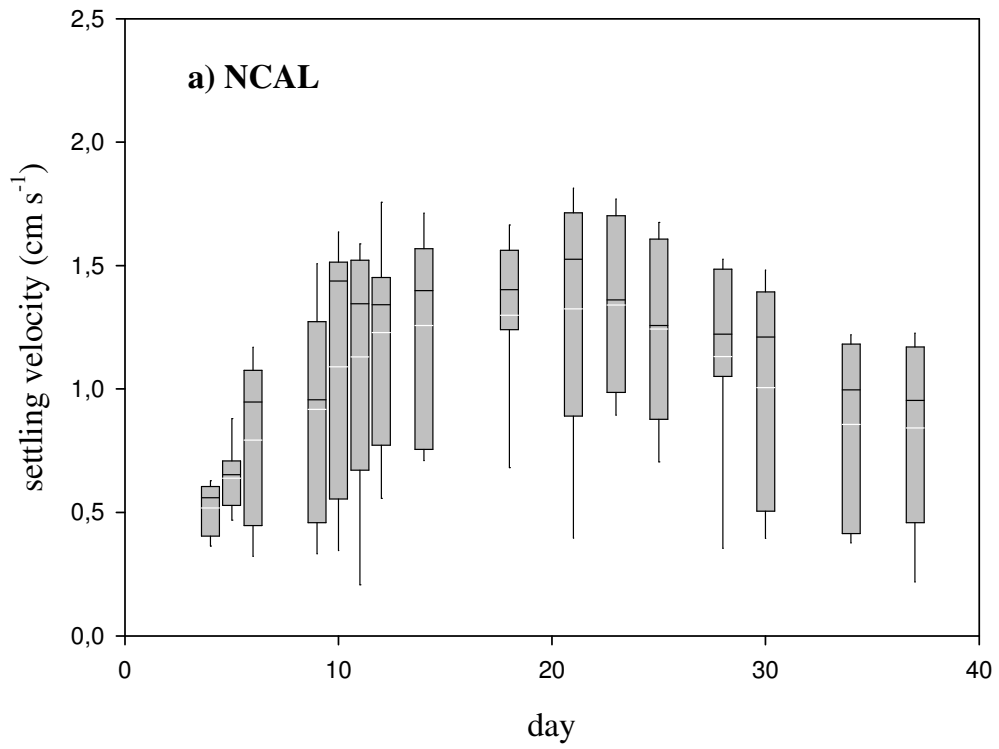
929

930

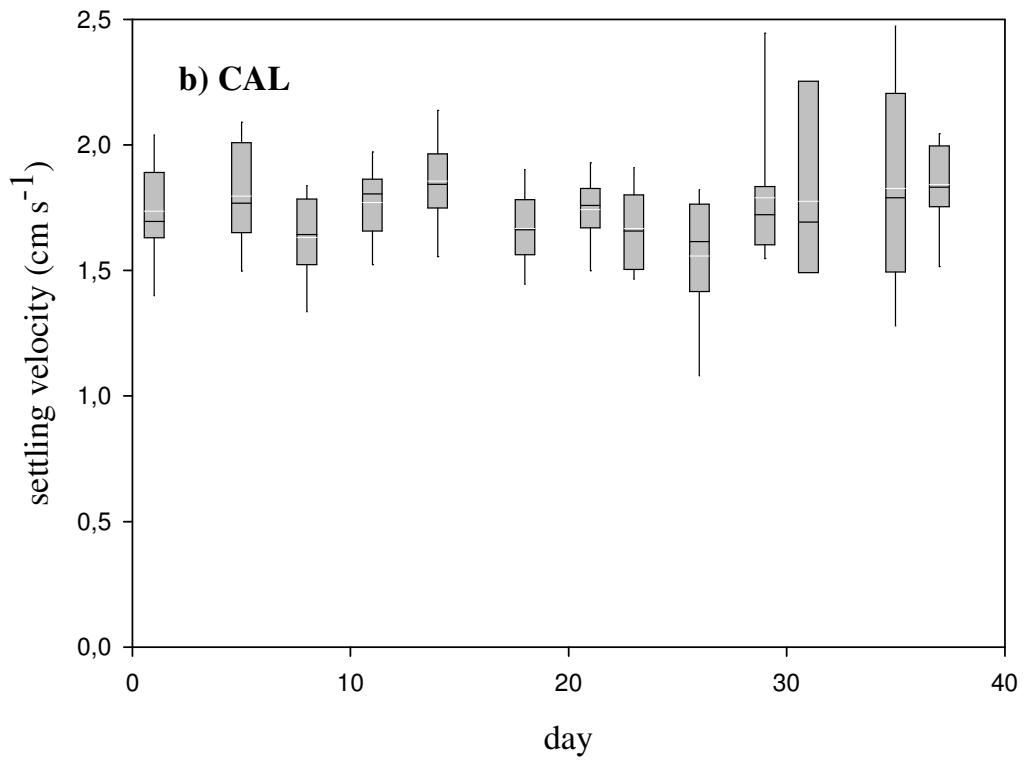
931

932

Engel et al., Figure 3a, b



933

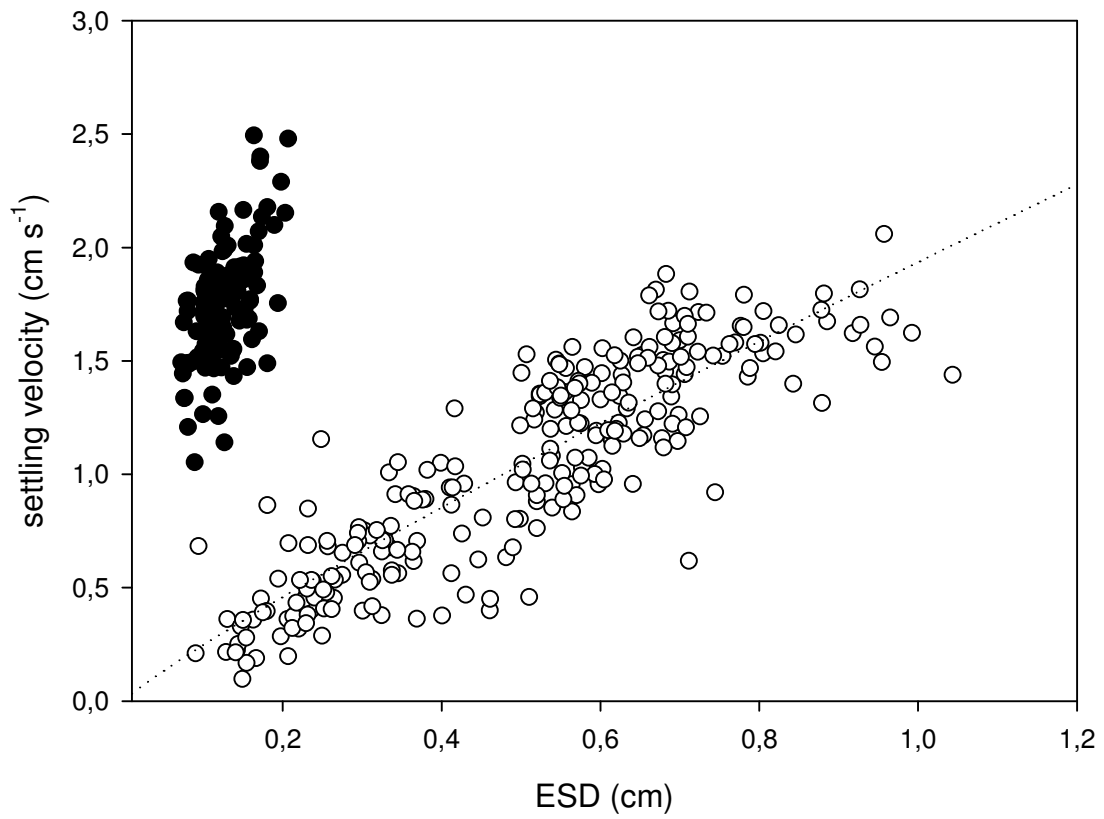


934

935

936

Engel et al. Figure 4a,b

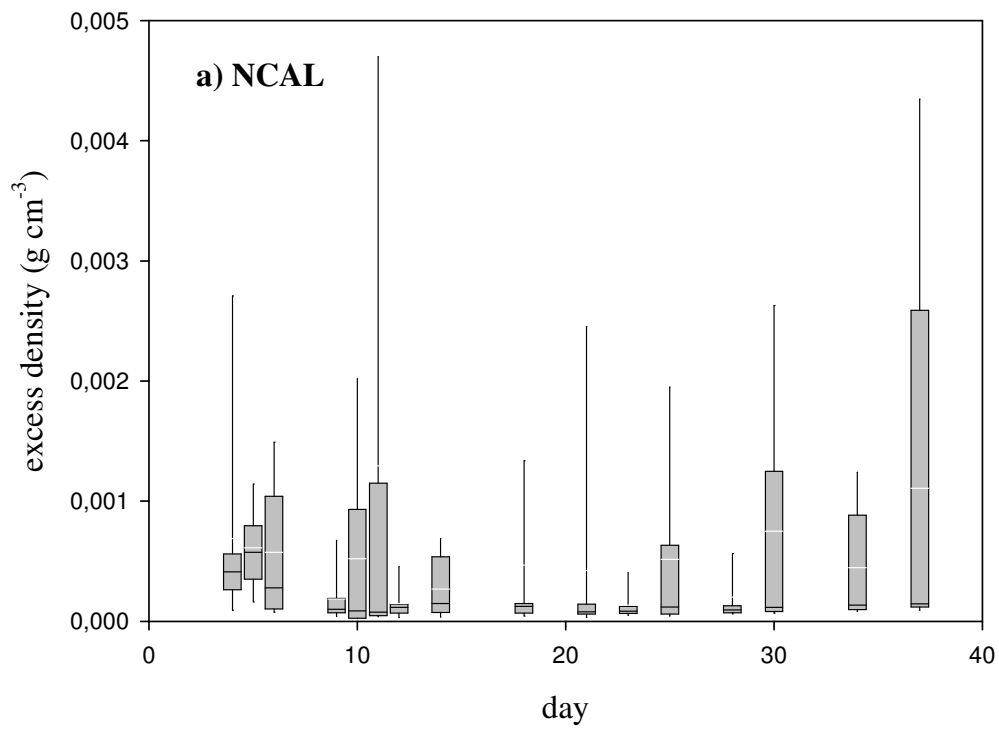


937

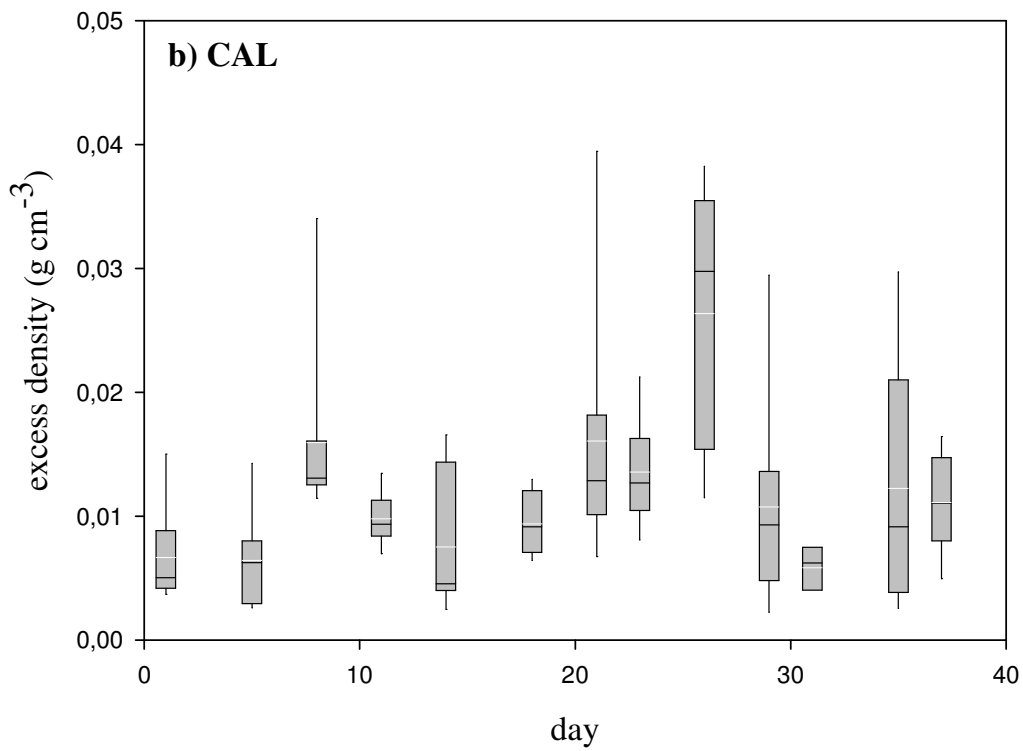
938

939

Engel et al., Figure 5



940

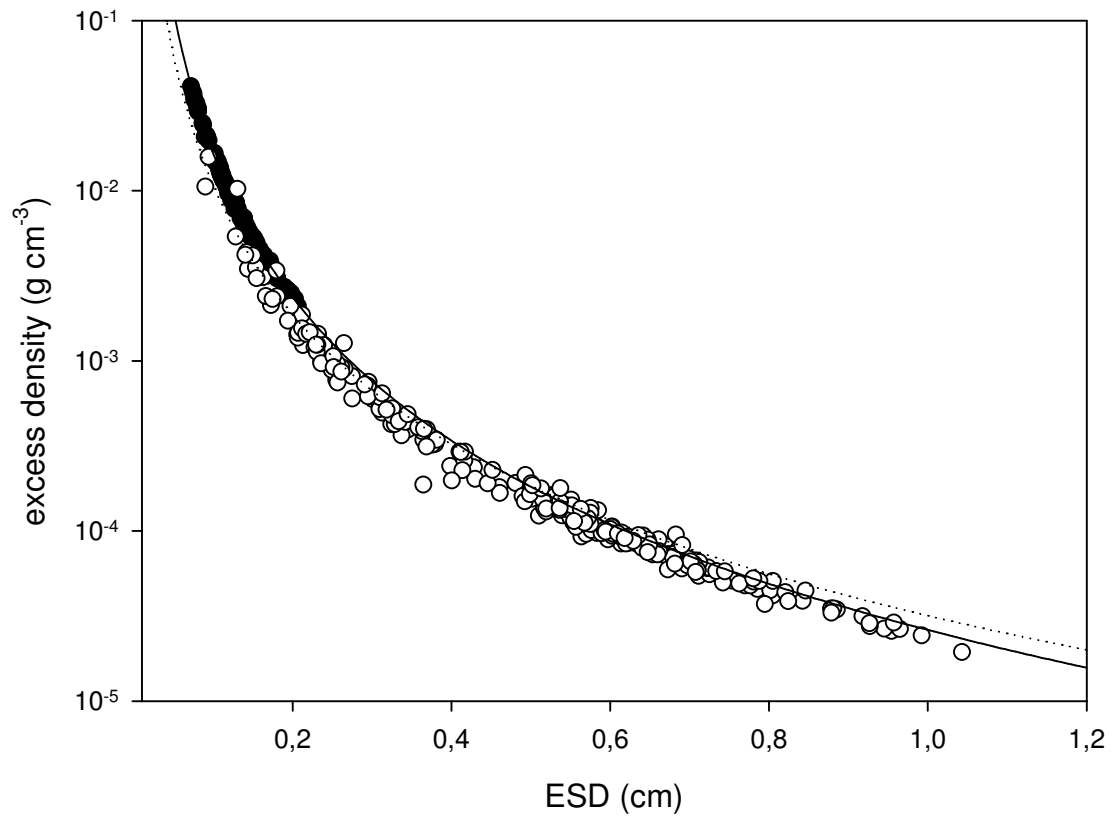


941

942

Engel et al., Figure 6 a, b

943



944

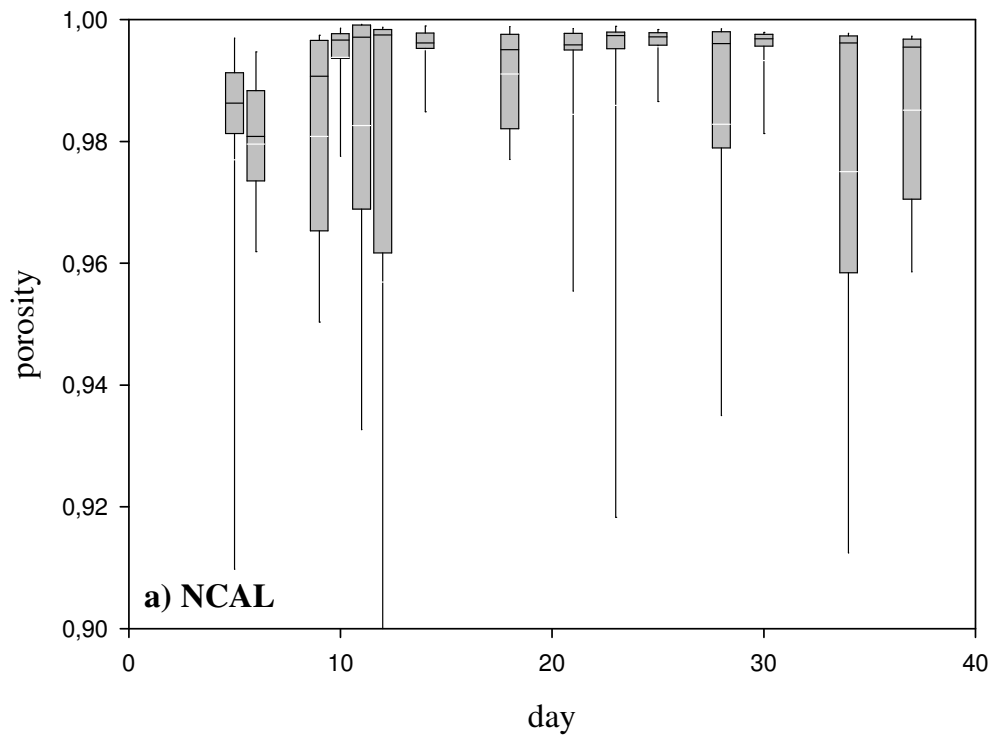
945

946

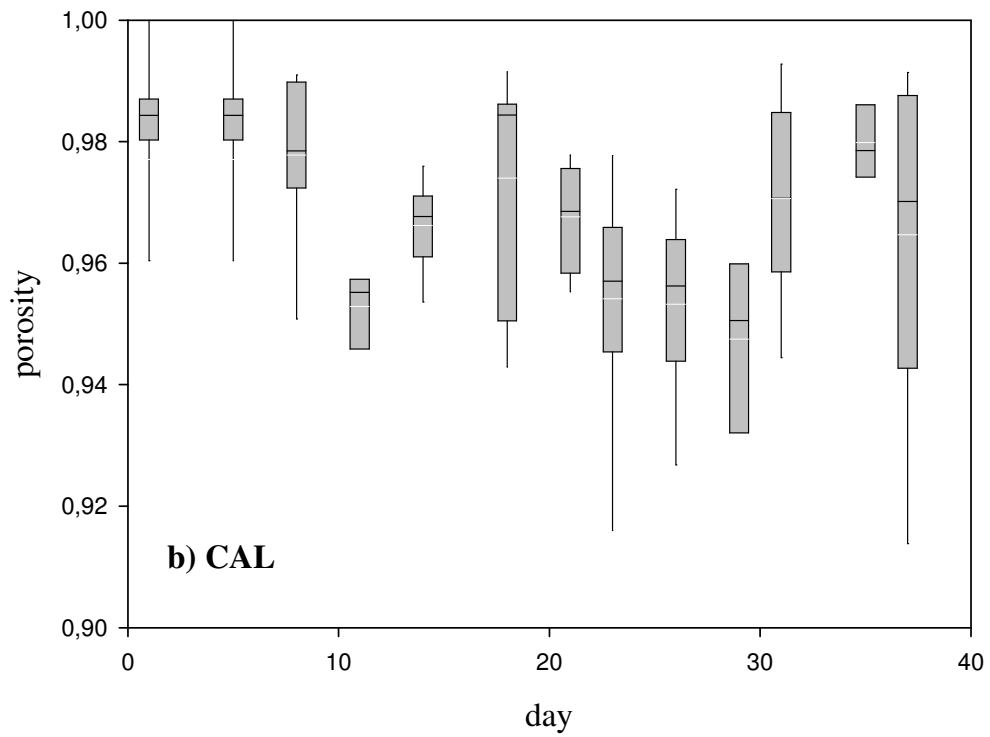
947

948

Engel et al. Figure 7



949

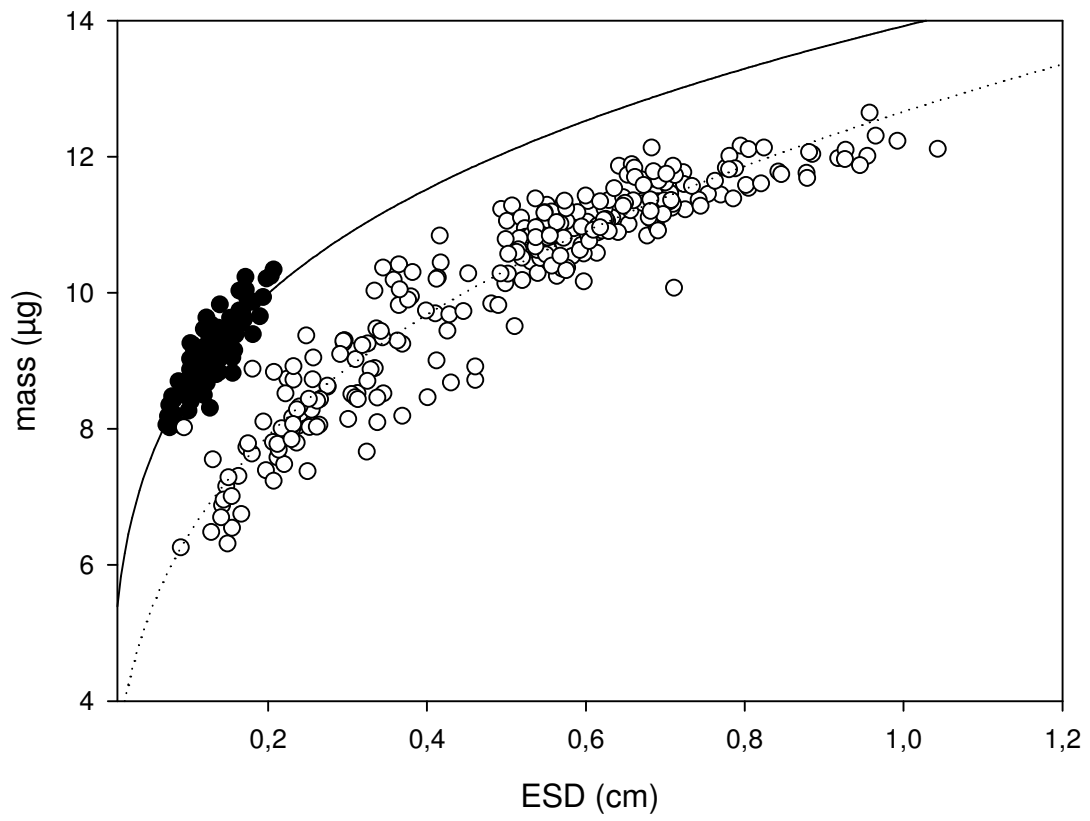


950

951

952

Engel et al. Figure 8a, b



953

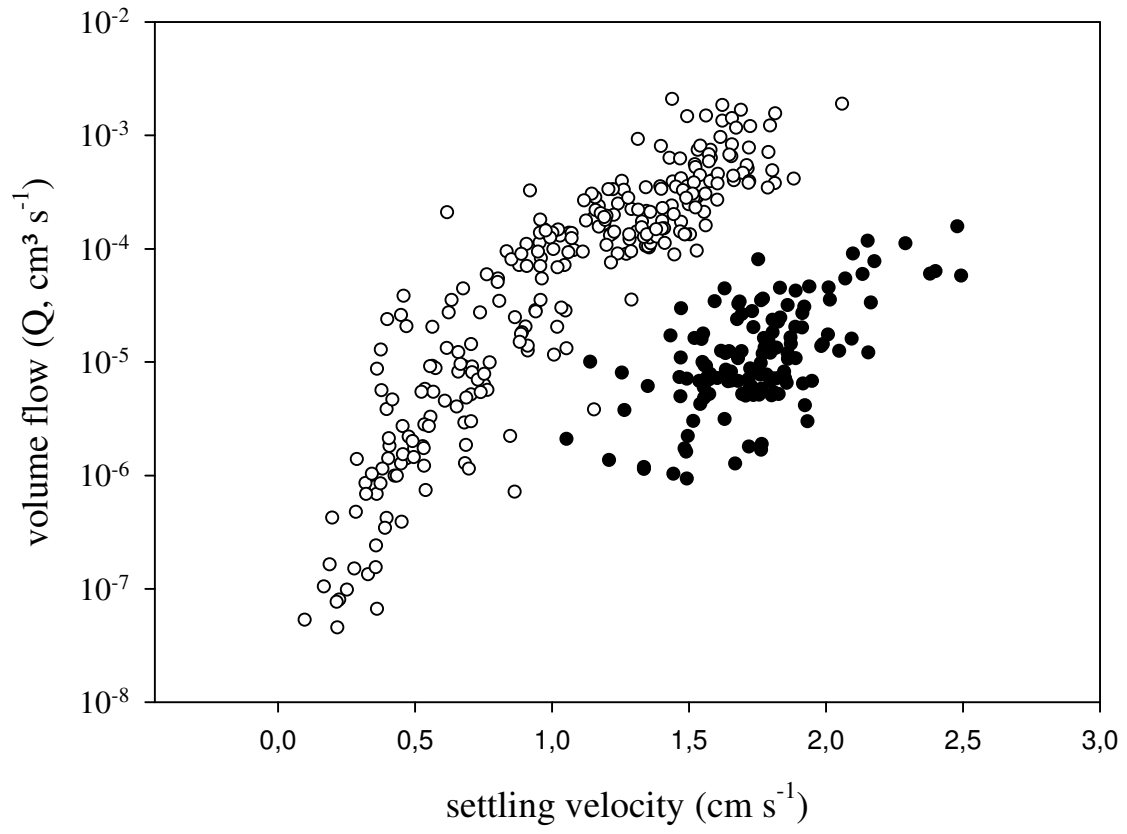
954

955

956

Engel et al. Figure 9

957

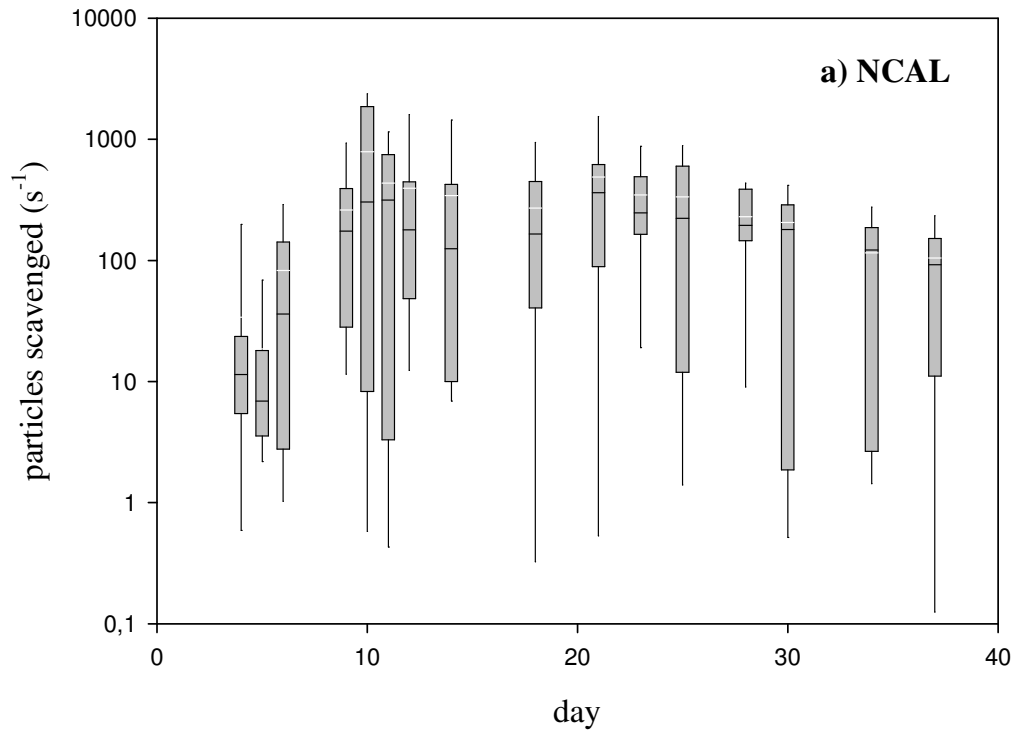


958

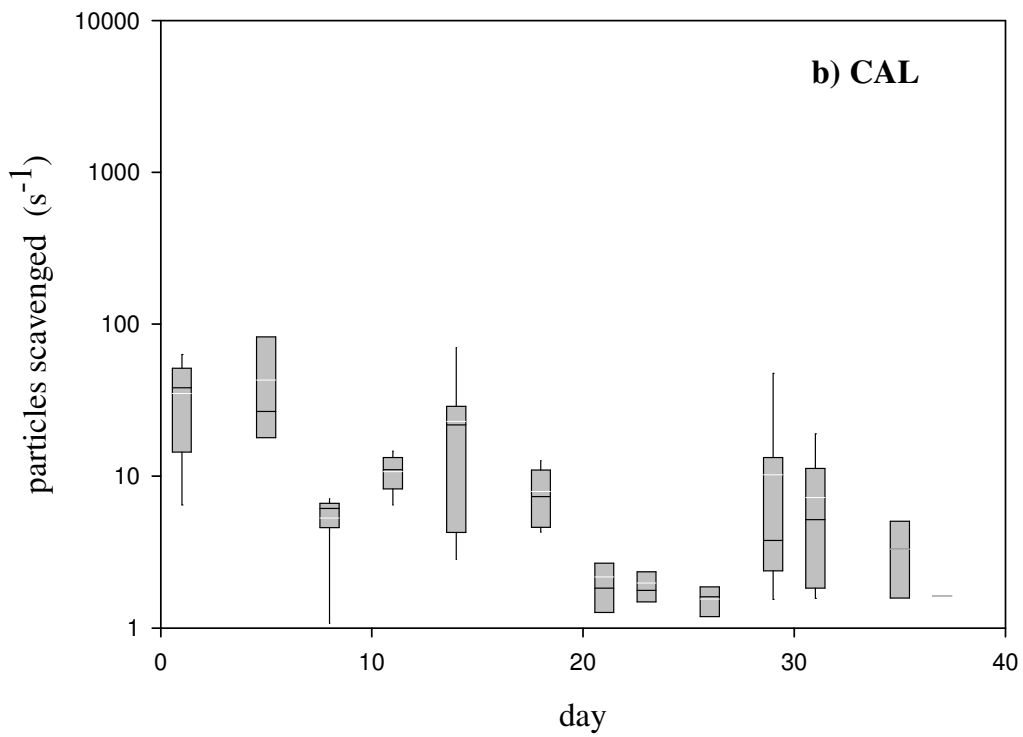
959

960

Engel et al. Figure 10



961



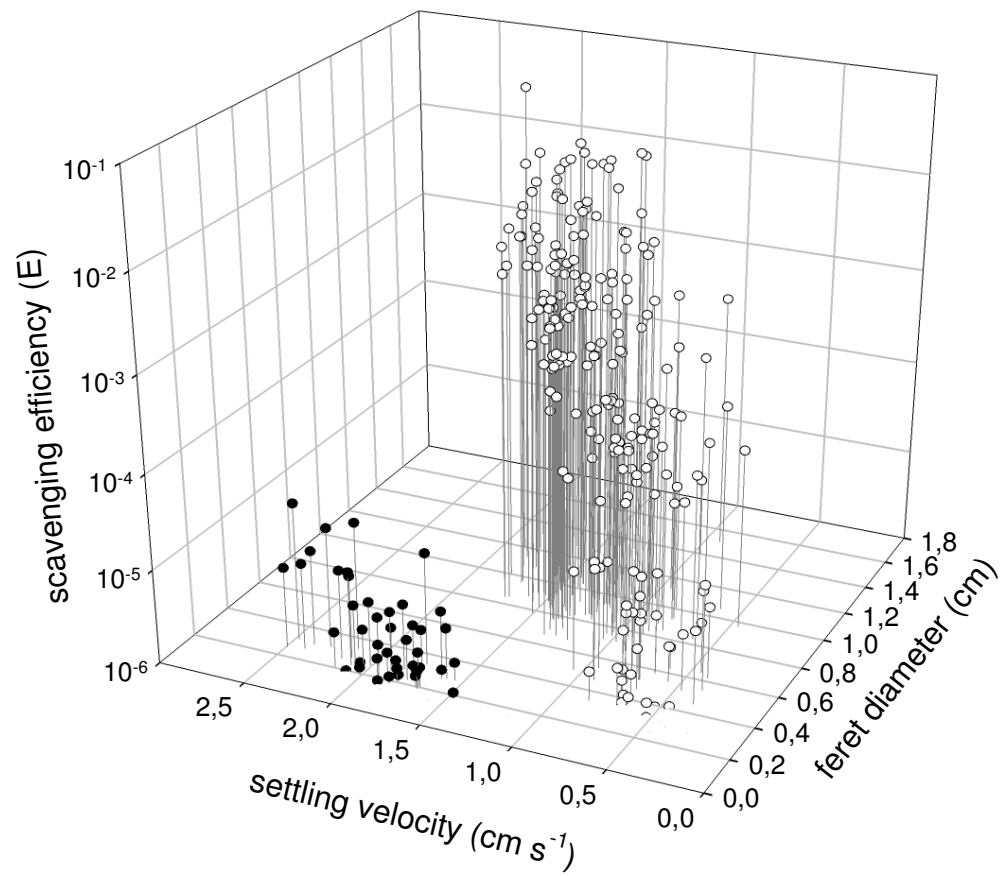
962

963

964

Engel et al. Figure 11a,b

965



966

967

968

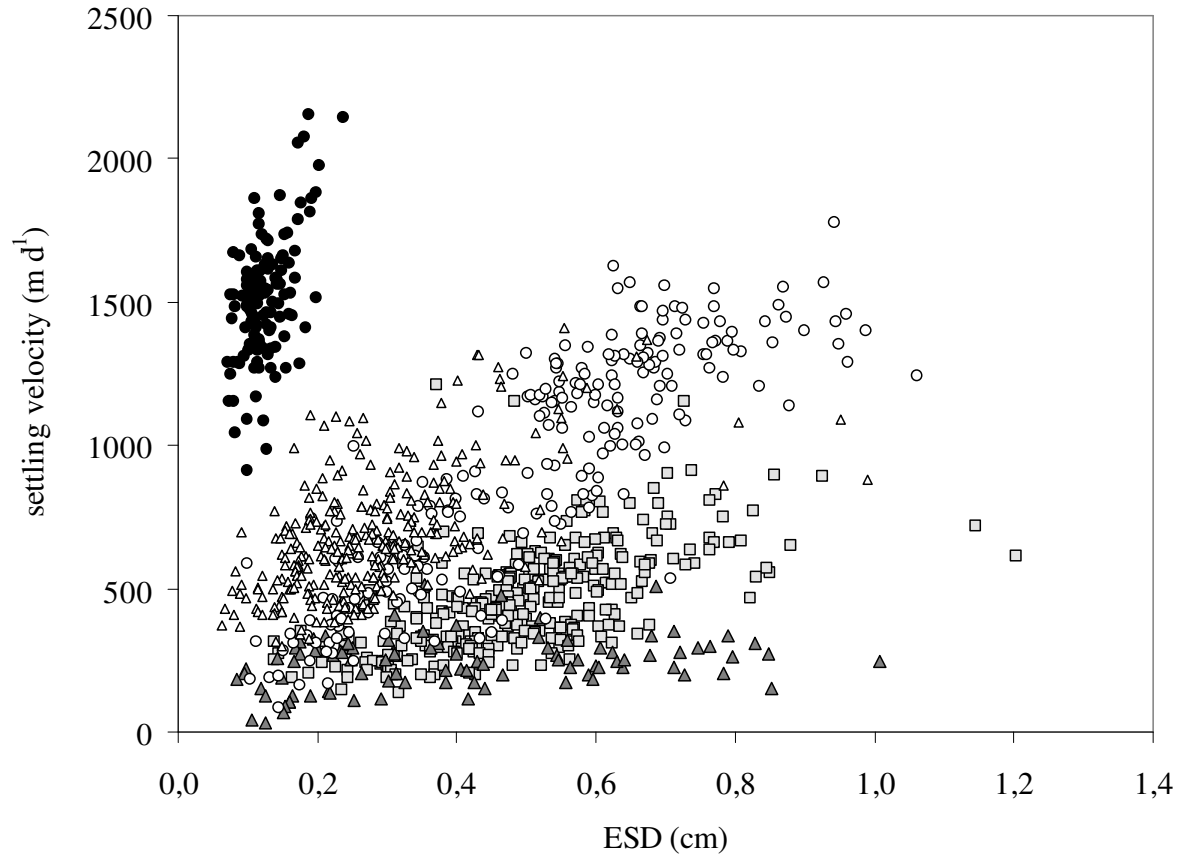
969

Engel et al. Figure 12

970

971

972



973

974

975

Engel et al., Figure 13

976